AD-A166 376 A STUDY OF ULTRAVIOLET EMISSIONS FROM THE OXIDES OF CARBON IN THE MESOSPHERE AND SHUTTLE ENVIRONMENT(U) AIR FORCE INST OF TECH WRIGHT-PATTERSON AFB OH R P TOMIC 1/1

UNCLASSIFIED 1985 AFIT/CI/NR-86-4T F/G 7/5 NL

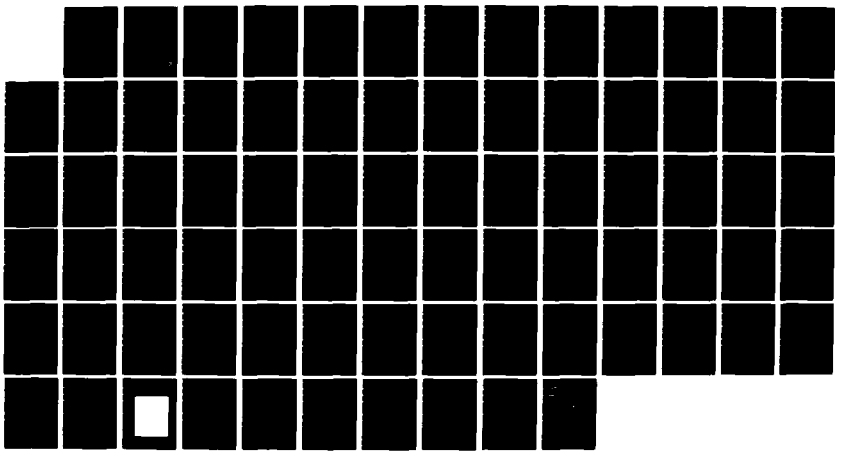

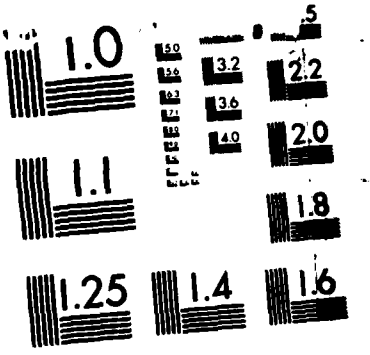

SECURITY CLASSIFICATION OF THIS PAGE (When Data Entered)

REPORT DOCUMENTATION PAGE

READ INSTRUCTIONS BEFORE COMPLETING FORM

1. REPORT NUMBER: AFIT/CI/NR 86-4T
2. GOVT ACCESSION NO.
3. RECIPIENT'S CATALOG NUMBER

4. TITLE (and Subtitle): A Study of Ultraviolet Emissions from the Oxides of Carbon in the Mesosphere and Shuttle Environment
5. TYPE OF REPORT & PERIOD COVERED: THESIS/DISSERTATION
6. PERFORMING ORG. REPORT NUMBER

7. AUTHOR(s): Robert P. Tomic
8. CONTRACT OR GRANT NUMBER(s)

9. PERFORMING ORGANIZATION NAME AND ADDRESS: AFIT STUDENT AT: Utah State University
10. PROGRAM ELEMENT, PROJECT, TASK AREA & WORK UNIT NUMBERS

11. CONTROLLING OFFICE NAME AND ADDRESS: AFIT/NR, WPAFB OH 45433-6583
12. REPORT DATE: 1985
13. NUMBER OF PAGES: 68

14. MONITORING AGENCY NAME & ADDRESS(if different from Controlling Office)
15. SECURITY CLASS. (of this report): UNCLASS
15a. DECLASSIFICATION/DOWNGRADING SCHEDULE

16. DISTRIBUTION STATEMENT (of this Report)

APPROVED FOR PUBLIC RELEASE; DISTRIBUTION UNLIMITED

17. DISTRIBUTION STATEMENT (of the abstract entered in Block 20, if different from Report)

18. SUPPLEMENTARY NOTES

APPROVED FOR PUBLIC RELEASE: IAW AFR 190-1

LYNN E. WOLAVER 4 Apr 86
Dean for Research and Professional Development
AFIT/NR, WPAFB OH 45433-6583

19. KEY WORDS (Continue on reverse side if necessary and identify by block number)

20. ABSTRACT (Continue on reverse side if necessary and identify by block number)

DD FORM 1 JAN 73 1473 EDITION OF 1 NOV 65 IS OBSOLETE

SECURITY CLASSIFICATION OF THIS PAGE (When Data Entered)

ABSTRACT

A Study of Ultraviolet Emissions From the
Oxides of Carbon in the Mesosphere and
Shuttle Environment

by

Robert P. Tomic, Master of Science
Utah State University, 1985

Committee Chairman: Dr. Marsha R. Torr
Major Professor: Dr. Gene L. Wooldridge
Department: Biometeorology

This ~~is a~~ study to determine if carbon oxide (CO, CO_4^+, CO_2^+) ultraviolet ~~(UV)~~ emissions in the mesosphere are observable, thus presenting an alternate method of determining the concentrations of these species. By developing photochemical models for CO_4^+ and CO_2^+ it is shown that the concentration levels of CO_4^+ and CO_2^+ are not adequate to produce UV band emissions bright enough to be detectable by spectrometric instruments. For CO, actual measurements of the concentrations were used in conjunction with g-factors to predict volume emission rates. These predictions indicate that only the CO fourth positive bands will be bright enough to measure by optical techniques.

Mesospheric ultraviolet spectra obtained by the Imaging Spectrometric Observatory (ISO) on the Spacelab 1 Mission (November 28-December 7, 1983) are examined for the presence of

the CO fourth positive bands and several bands are identified which are believed to be CO fourth positive. The CO fourth positive 1-6 band is used to calculate a density height profile for mesospheric CO. These calculations are in close agreement with measurements by others for mesospheric CO. This band system ~~does~~ provides a viable method for measuring CO in the 80 km to 110 km altitude region.

A second (study) objective ~~of the study~~ is to investigate whether carbon oxide emissions are found in the induced shuttle environment. CO_2^M is one of the major products of shuttle engine exhaust and carbon materials are found to undergo significant mass loss on orbit. While several molecular band-like features are found in the data, these appear to be intermittent and at times have the characteristics of point sources, and so may ~~These features~~ may therefore be due to particulates or stars rather than exhaust plumes. Keywords: Ultraviolet spectra, Photochemistry, Daytime. -1-

(76 pages)

A STUDY OF ULTRAVIOLET EMISSIONS FROM THE OXIDES

OF CARBON IN THE MESOSPHERE AND

SHUTTLE ENVIRONMENT

by

Robert P. Tomic

A thesis submitted in partial fulfillment
of the requirements for the degree

of

MASTER OF SCIENCE

in

Soil Science and Biometeorology

(Biometeorology)

Approved:

Committee Chairman

Major Professor

Committee Member

Dean of Graduate Studies

UTAH STATE UNIVERSITY
Logan, Utah

1985

ACKNOWLEDGMENTS

A special thanks is extended to Dr. Marsha Torr for her guidance and support throughout the course of this study. I also wish to thank Dr. Lawrence Hipps and Dr. Gene Wooldridge for their friendship and help over the last two years. Thank you Amy Krambule for your patience in the typing and retyping of this thesis. And finally to my wife, Judy; my children, Leslie and Candice; and my parents, without whose love none of this would be possible, thank you.

Robert P. Tomic

TABLE OF CONTENTS

LIST OF TABLES

LIST OF FIGURES

LIST OF FIGURES CONTINUED

INTRODUCTION

Studies of carbon oxide (CO, CO_2, CO^+, CO_2^+) ultraviolet (UV) emissions in airglow have been used extensively to study atmospheres on planets such as Mars (Conway, 1981; Fox and Dalgarno, 1979; Barth et al., 1971), Venus (Durrance, 1981) and comets (Feldman, 1978; Festou et al., 1982; Donn et al., 1974; Feldman and Brusil, 1976). In this study, an attempt was made to determine if carbon oxide UV emission could be detected in the earth's atmospheric dayglow and the shuttle's induced glow. If detectable, this will be the first case in which carbon oxide UV emissions from mesospheric dayglow have ever been remotely measured. This is very important because it will be an excellent tool to aid in the study of mesospheric physical processes.

For the purpose of this paper, the mesosphere is the region of the atmosphere ranging in altitude from 88 km to 116 km. Figure 1 shows where the mesosphere lies in relation to the other atmospheric layers (thermosphere, stratosphere and troposphere) and which portion of the solar spectra is absorbed out in the mesosphere (2000 to 3000 Å). This includes most of the E region of the ionosphere which is dominated by the ions NO^+ and O_2 . More measurements of this region will aid in understanding the transport processes, photochemistry and ionospheric phenomena such as sporadic E.

By comparison with the thermosphere, relatively little is actually known about mesospheric processes because it is a very

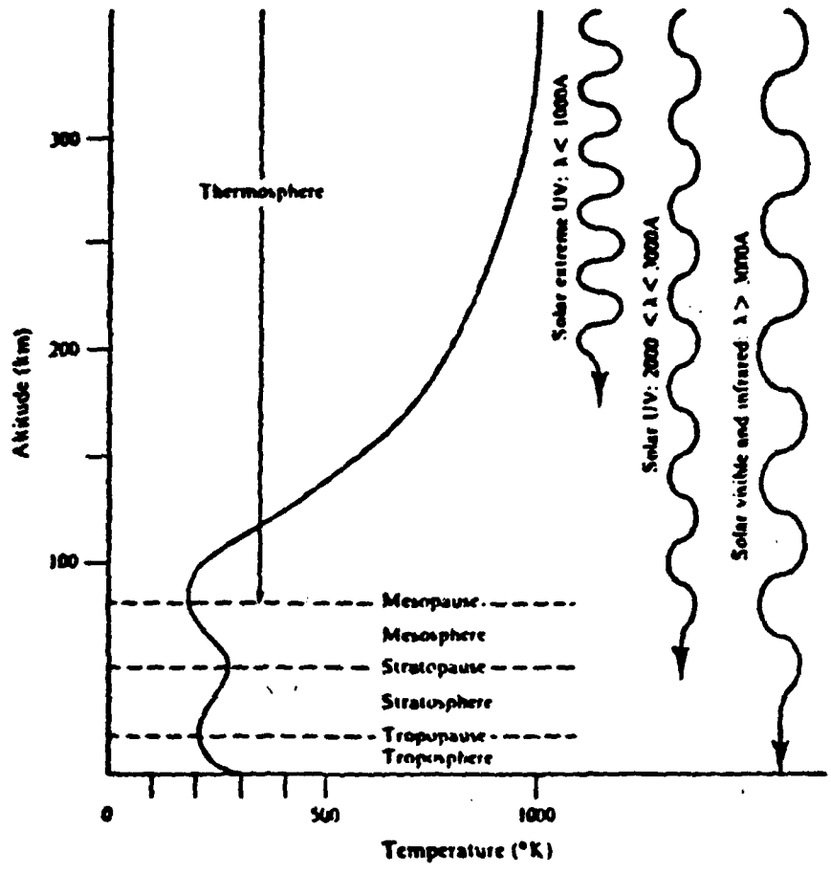

Figure 1. The variation of temperature with altitude at middle latitudes in the earth's atmosphere (Goody and Walker, 1972).

difficult portion of the atmosphere from which to collect data. Until recently, the collection of data was done primarily with rockets. This resulted in a scattered picture of processes by which the mesosphere operates physically. In 1983 mesospheric carbon oxides were measured by an infrared instrument on board Spacelab I (Lippens et al., 1984). The purpose of measuring carbon oxides is to gain a greater understanding of the physical and chemical processes which drive the mesosphere. This includes the carbon oxide rotational and vibrational population distribution, photochemistry, mesospheric temperature and solar and magnetospheric energy flux (Torr and Torr, 1984).

In order to examine the data for mesospheric carbon oxide emissions (in the UV) it is important to first predict theoretically where these lines will occur, and how bright the emissions should be. Because brightness is a function of species concentration (shown later) a photochemical model is developed which determines concentration levels for both CO^+ and CO_2^+ (assuming photochemical equilibrium). For CO and CO_2 this assumption does not hold true (Hays and Olivero, 1970). Therefore, actual measurements (taken on Spacelab I) will be used in place of predicted concentrations. These concentration values are then used to predict how bright several of the carbon oxide bands should be. The second step involves locating where these emission lines occur. This was done using a synthetic spectral model. Once estimated brightness values and band locations are known, the final step can be taken, which involves the comparison of the actual data (band brightness and

location) to the predicted band brightness and locations. This same process is used when studying carbon oxide UV emission bands associated with shuttle induced glow. This induced glow is the measurement of extraneous signals whose origin seems uncertain at this time (Murad, 1985). There are three suggested causes for production of this glow, which include aeronomical processes, plasma effects, and gaseous contaminants from the shuttle.

INSTRUMENTATION AND DATA REDUCTION

Data obtained for this thesis were measured by the Imaging Spectrometric Observatory (ISO) on board Spacelab I from 28 November to 7 December 1983. The ISO was built to measure emission features in the ultraviolet, visible and near infrared (300 to 12,700 Å). This is achieved through "five spectrometers operating in parallel" each having "a focal plane detector which is optimized for a particular region of the full spectral range" (Torr and Torr, 1984, p. 169). Each spectrometer measures approximately equal portions of the spectrum from the 300 Å to 12,700 Å range with a spectral resolution of 3 to 6 Å (Torr et al., 1982). See Figure 2 for a diagram of the ISO and its ray path description. The focal-plane detectors consist of a "two dimensional device array" which measures UV spectral emission (via grating steps) in one dimension and spatial information in the other dimension (Torr and Torr, 1984, p. 169).

By positioning the shuttle's instrumentation in the proper orientation, a vertical height profile of UV emissions in the day and nightglow can be collected. The dayglow measurements were obtained by orienting "the entrance slit perpendicular to the limb of the earth" (Torr and Torr, 1984, p. 169). The ISO's field of view of 0.65° allows a 16 km vertical height profile (with a 2 km resolution) to be observed (Torr et al., 1982). The measurements for shuttle glow were taken on the night side of the orbit. The shuttle was

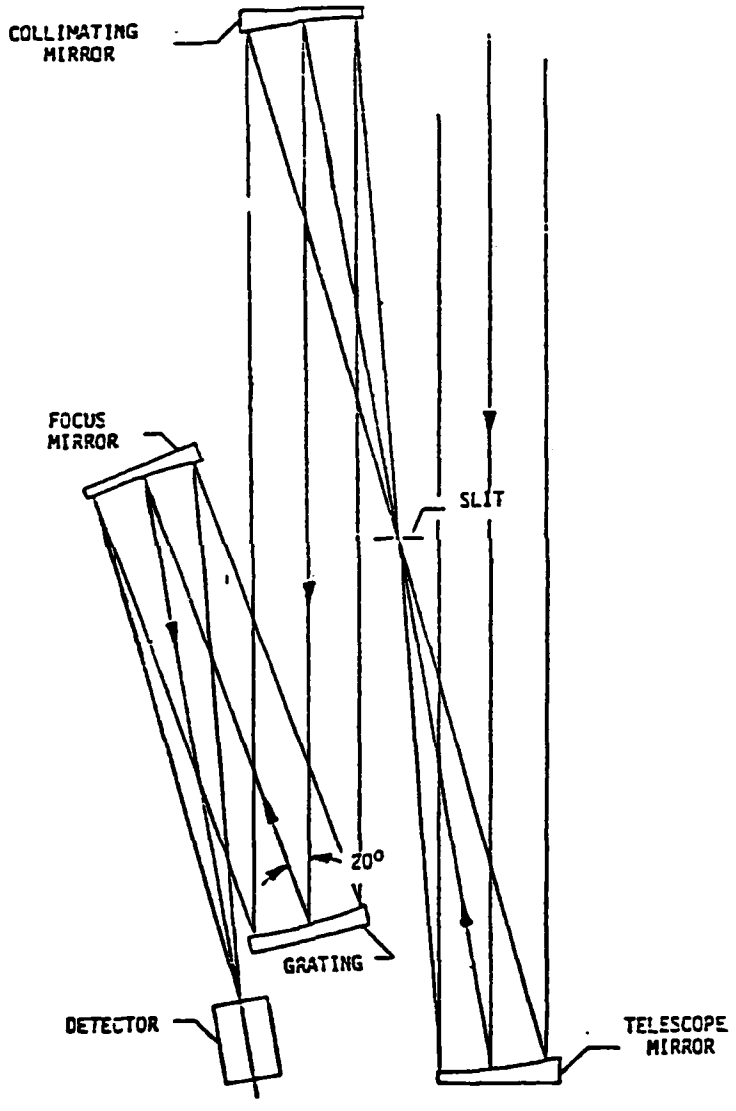

Figure 2. Optical configuration of the imaging spectrometers for wavelengths longward of 1200 Å (Torr et al., 1982).

oriented so that the ISO pointed at a tangent ray height of 90 km.

The data collected was recorded on magnetic tape by a microprocessing computer on board Spacelab I. Processing this data involved four steps. The first step required the use of a program developed on the PDP 11/60 and PDP 11/34 computer at Utah State University. This program, called SPY, has the capability to extract the data in two formats. The data can be either in one dimension centered at the tangent ray height or in eight segments (every two kilometers) centered at the tangent ray height. This results in a height profile which extends eight kilometers above and below the tangent ray height. Because the sensor contains background noise, an instrument background measurement is taken before the ISO shutters are opened for observations. This is then subtracted from the data using a prepackaged program at the ISO Laboratory at Utah State University (CAL 2). The third step involves cleaning the data by removal of telemetry noise spikes and aligning each section of the spectra to the other. With the spectra fairly well cleaned, the data must be converted from counts to radiance. A calibrated sensitivity file is used to do this conversion. Figure 3 shows an example of the final output form for the one dimension data extraction technique.

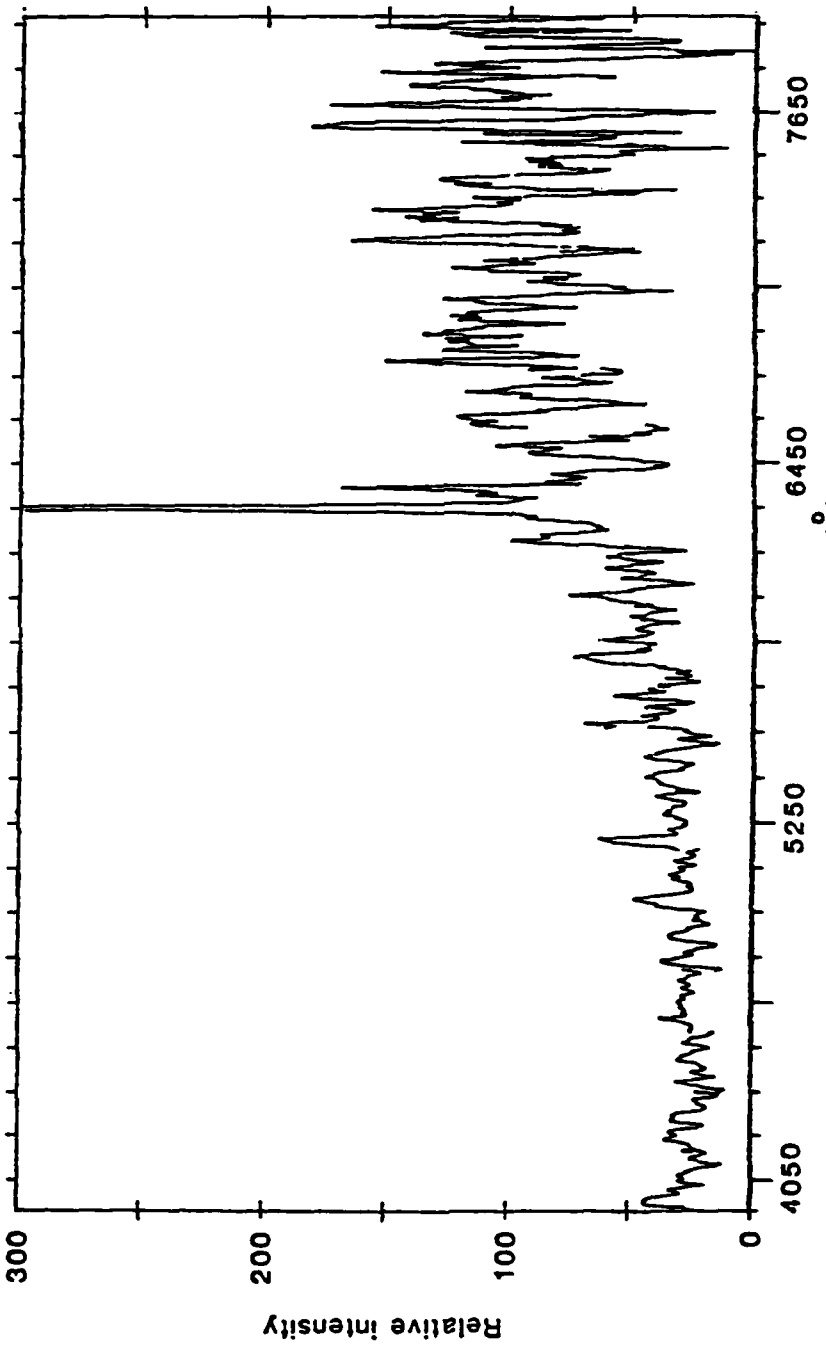

Figure 3. Condensed display of spectrum acquired by visible channel during a period of observations into the velocity vector (Torr and Torr, 1984).

SYNTHETIC SPECTRAL MODEL

To study the data collected on Spacelab I for carbon oxide UV emissions, it is necessary to know the expected location of each band. This requires a large number of calculations which consider the contribution from each of the atomic and rotational lines to the spectrum. Therefore, it is advantageous to utilize a computer model which can do this.

The model used in this paper titled "Line by Line Calculation of Spectra From Diatomic Molescules and Atoms Assuming a Voigt Line Profile" was developed by Arnold, Whiting and Lyle (1969, p. 1).

> The program produces a spectrum by accounting for the contribution of each rotational and atomic line considered. The integrated intensity of each line is distributed in the spectrum by an approximate Voigt profile. (Whiting et al., 1969, p. 1)

According to Arnold et al. (1969, p. 783), using the Voigt line profile is "accurate to within 3 percent or less." Another important aspect of this model is the capability to incorporate instrument sensitivity. This allows modeled output to actually appear as it would when measured by an instrument with specific sensitivity characteristics (grating spectrometer, radiometer, etc.). For more information reference Arnold et al. (1969) and Whiting et al. (1969).

This model only considers atoms and diatomic molecules, therefore only CO and CO^+ emission bands were modeled. The

input variables which can affect the CO and CO^+ emission band calculations are:

1. rotational, vibrational and electron temperatures;
2. species concentration;
3. instrument sensitivity; and
4. population distribution which can be modified to consider vibrational distribution.

Figures 4 through 8 show the brighter calculated emission lines for the following CO and CO^+ UV bands:

CO: Fourth Positive Bands (Fig. 4)
Cameron Bands (Fig. 5)
Hopfield-Birge Bands (Fig. 6)

CO^+: First Negative Bands (Fig. 7)
Comet Tail Bands (Fig. 8)

In these figures, a thermal distribution of the vibrational and rotational states has been assumed. The actual atmospheric excitation mechanisms might well result in different population distributions. These bands were utilized because they reside in the portion of the spectrum the ISO can observe, and all of the necessary molecular constants had been calculated or measured. These plots are then used to aid in identifying actual lines in the next and final step of analyzing the ISO data.

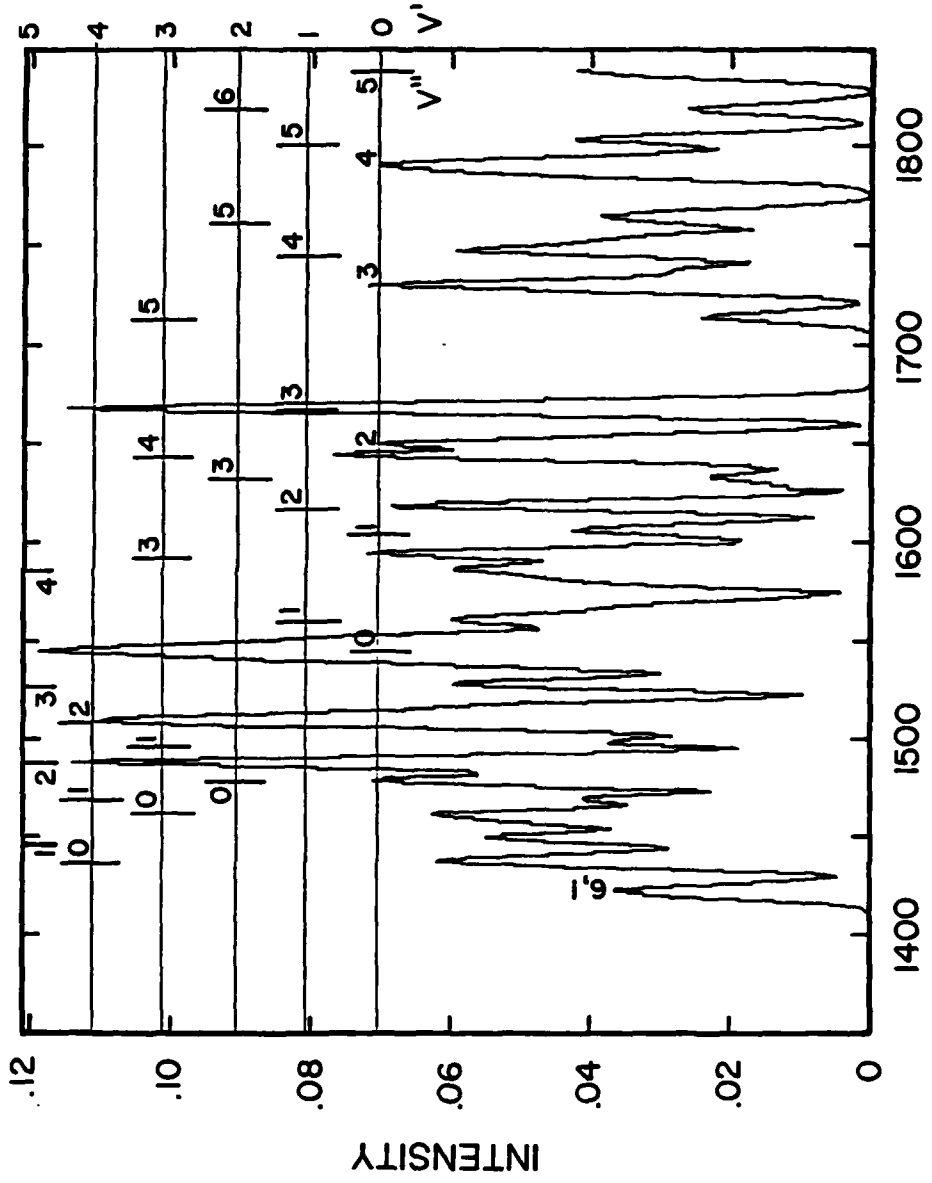

Figure 4. Synthetically produced CO Fourth Positive bands.

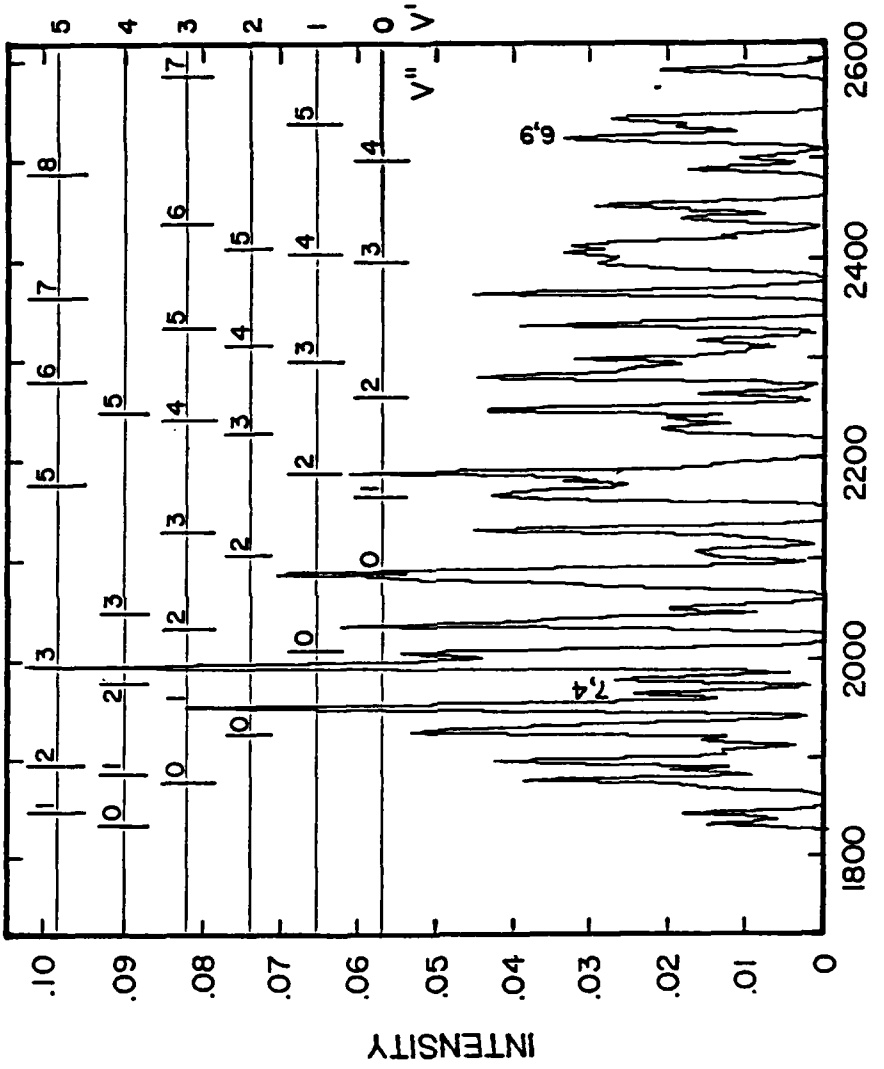

Figure 5. Synthetically produced CO Cameron bands.

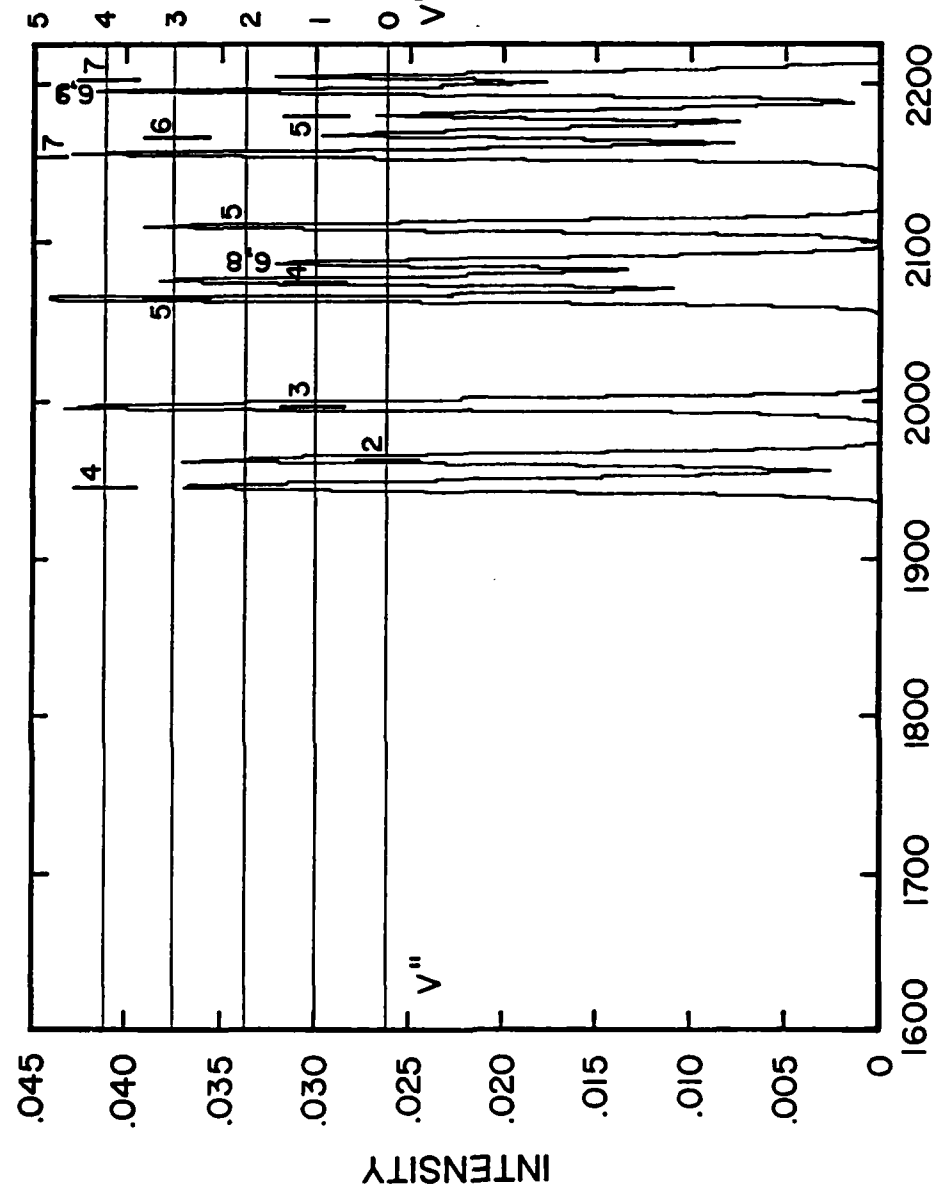

Figure 6. Synthetically produced CO Hopfild-Birge bands.

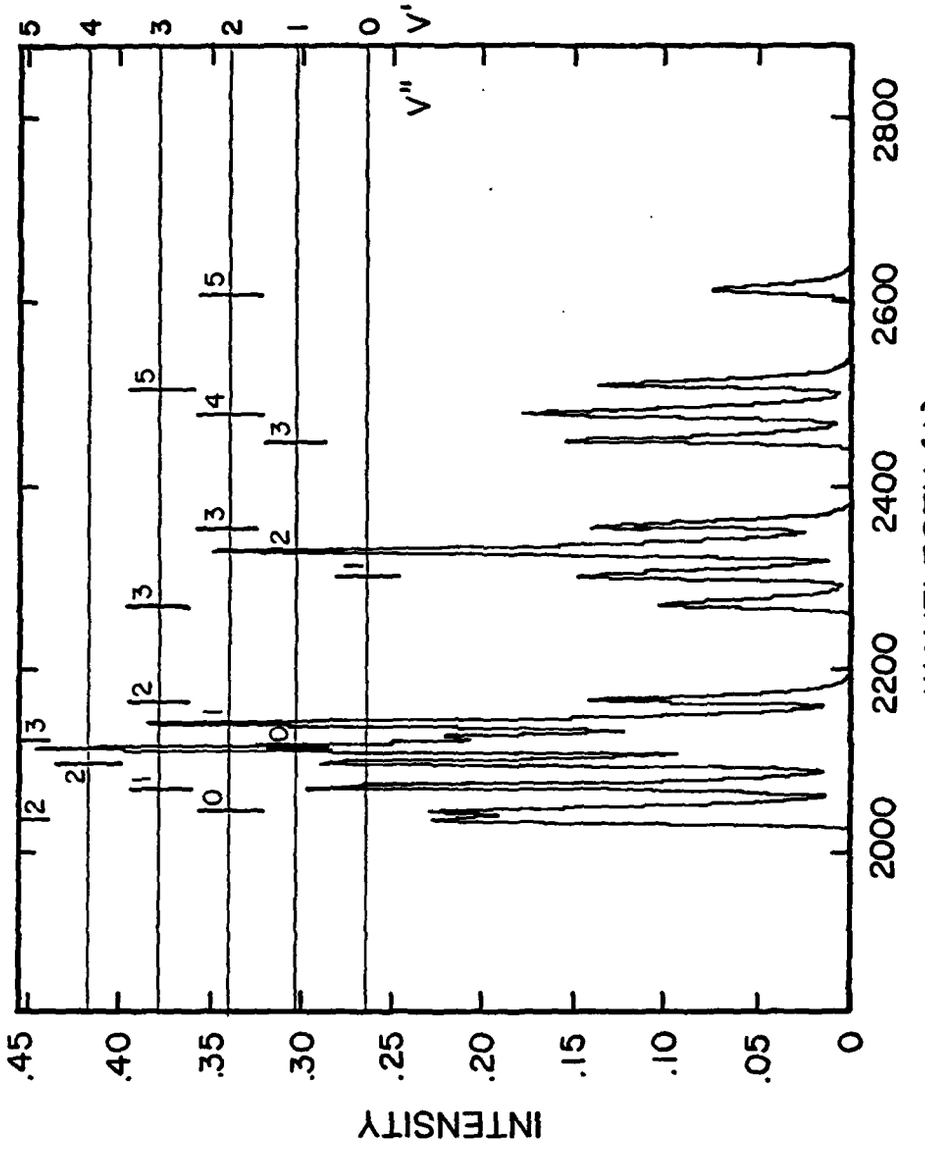

Figure 7. Synthetically produced CO^+ First Negative bands.

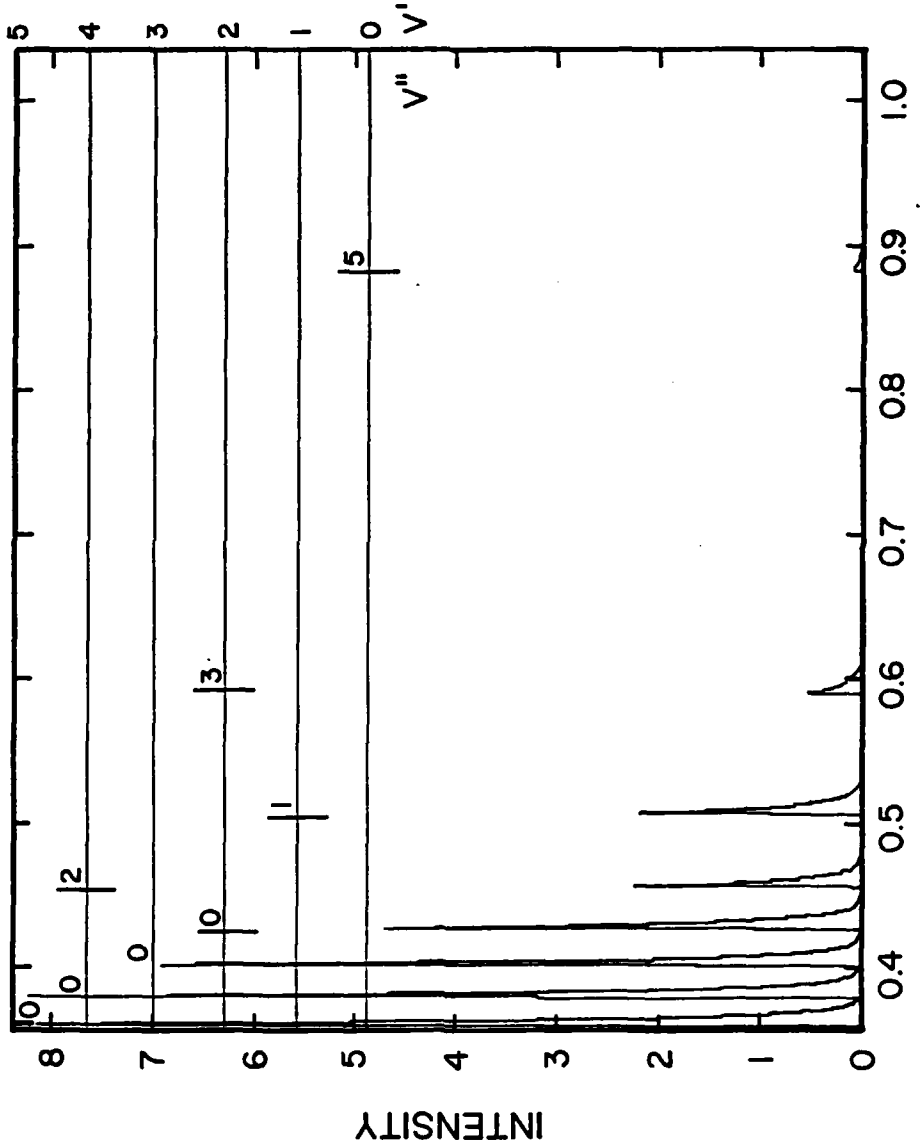

Figure 8. Synthetically produced CO^+ Comet Tail bands.

PHOTOCHEMISTRY AND BRIGHTNESS CALCULATIONS

In order to predict theoretical intensity profiles for carbon oxide UV emission there is a need to understand the carbon oxide photochemical processes. The photochemical processes control how some of the carbon oxides (CO^+, CO_2^+) distribute themselves with altitude (Hays and Olivero, 1970). The other carbon oxides (CO, CO_2) distribute themselves via transport processes in the mesosphere (Lippens et al., 1984). As will be shown, the concentration profiles with height of CO^+, CO_2^+, CO and CO_2 are needed to calculate the vertical carbon oxide intensity profiles.

The techniques used to determine the height profiles for CO and CO_2 are quite different from those used to find height profiles for CO^+ and CO_2^+. The reason for this is the unknown physical processes which control mesospheric CO^+ and CO_2^+. It is common for a first theoretical prediction to assume photochemical equilibrium for unknown constituents (CO^+ and CO_2^+). However, for mesospheric CO and CO_2 this assumption is not true according to Hays and Olivero (1970).

Even though CO and CO_2 are not in photochemical equilibrium a height profile of each constituent is needed. The best approach appears to be the use of actual data collected by an infrared grille spectrometer which was flow aboard Spacelab I along with the ISO. Therefore, the CO and CO_2 concentration profiles are taken from the findings of Lippens et al. (1984).

The calculation of CO^+ and CO_2^+ height profiles is performed under the assumption of photochemical equilibrium. Through an extensive literature search the author collected known photochemical equations involving CO^+ and CO_2^+ for the earth's atmosphere (M. Torr, 1985) and the martian atmosphere (M. Torr, 1985; Fox and Dalgarno, 1979; Yung et al., 1971). Many of the photochemical equations were not considered for the following possible reasons:

1. One or more of the constituents used in the photochemical equation is not present in the earth's mesosphere.

2. The photochemical process was endothermic.

3. The concentration of one or more of the constituents in the photochemical equation was extremely small compared to larger atmospheric components used in the other considered photochemical equations.

4. The reaction rate coefficient was small enough that the contribution from the chemical process in question is quite small.

After applying these steps for the sources and sinks of CO^+ and CO_2^+, the following photochemical equations and rate coefficients were used for height profile calculations:

CO^+	Sources	$N_2^+ + CO \rightarrow N_2 + CO^+$	7.4×10^{-11} cm^{3}sec^{-1}
	Sinks	$CO^+ + O \rightarrow O^+ + CO$	1.4×10^{-10} cm^{3}sec^{-1}
		$CO^+ + CO_2 \rightarrow CO_2^+ + CO$	1.1×10^{-9} cm^{3}sec^{-1}
CO_2^+	Sources	$N_2^+ + CO_2 \rightarrow CO_2^+ + N_2$	9×10^{-10} cm^{3}sec^{-1}
	Sinks	$CO_2^+ + O_2 \rightarrow CO_2 + O_2^+$	5×10^{-11} cm^{3}sec^{-1}

Using the assumption of photochemical equilibrium allows the sources and sinks to be equated to each other. With this in mind the

following equation can be derived:

$$CO^+ \quad [N_2^+][CO]\ 7.4\times10^{-11}\ cm^3sec^{-1} = [CO^+][O]\ 1.4\times10^{-10}\ cm^3sec^{-1} + [CO^+][CO_2]\ 1.1\times10^{-9}\ cm^3sec^{-1}$$

$$CO_2^+ \quad [N_2^+][CO_2]\ 9\times10^{-10}\ cm^3sec^{-1} = [CO_2^+][O_2]\ 5\times10^{-11}\ cm^3sec^{-1}$$

where [X] represents the concentration of X. The solution for $[CO^+]$ and $[CO_2^+]$ involves simple algebraic manipulations. The end results are shown below:

$$[CO^+] = \frac{[N_2^+][CO]\ 7.4\times10^{-11}}{[O]\ 1.4\times10^{-10} + [CO_2]\ 1.1\times10^{-9}}$$

$$[CO_2^+] = \frac{[N_2^+][CO_2]\ 9\times10^{-10}}{[O_2]\ 5\times10^{-11}}$$

When available, the standard atmospheric density height profiles were used in the photochemical models described above. When they were not available, measurements were used. The height profiles used in the calculation for CO^+ and CO_2^+ are shown in Table 1. The results for CO^+ and CO_2^+ using the developed photochemical models are given in Table 2. By comparison to the other ions (O_2^+ and NO^+) present in this region of the atmosphere (Figure 9), both CO and CO_2^+ are insignificant. The concentrations for NO^+ ($10^4 cm^{-3}$) and O_2^+ ($3\times10^3 cm^{-3}$) are much larger than CO_2^+ ($< 1\ cm^{-3}$) and CO^+ ($< 1\ cm^{-3}$). As will be shown briefly, the concentration values of CO^+ and CO_2^+ are quite small and will not be large enough to produce observable UV emissions for the ISO to detect.

Intensity profile calculations predict the "probability that

Table 1. Concentration height profiles for N_2^+, CO, O, and CO_2.

Height (km)	Concentration ($cm^3 sec^{-1}$)			
	$[N_2^+]$(P1)	[CO](P2)	[O](P1)	$[CO_2]$(P2)
70	100	$3x10^9$	$1.5x10^{11}$	$6x10^{11}$
75	100	$1.7x10^9$	$1.8x10^{10}$	$2.8x10^{11}$
80	100	$8.2x10^8$	$1.8x10^{11}$	$1.2x10^{11}$
85	100	$5x10^8$	$7x10^{10}$	$5x10^{10}$
90	100	$4.5x10^8$	$2.8x10^{11}$	$1.8x10^{10}$
95	100	$4.5x10^8$	$5x10^{11}$	$4.5x10^9$
100	100	$2.3x10^8$	$8x10^{11}$	$2.5x10^9$

(P1) D. Torr (1985)
(P1) Lippens et al. (1984)

Table 2. Calculation concentration height profiles for CO^+ and CO_2^+.

Height (km)	Concentration ($cm^3 sec^{-1}$)	
	CO^+	CO_2^+
70	0.03	1
75	0.04	1
80	0.04	0.7
85	0.05	0.45
90	0.05	0.32
95	0.04	0.09
100	0.02	0.06

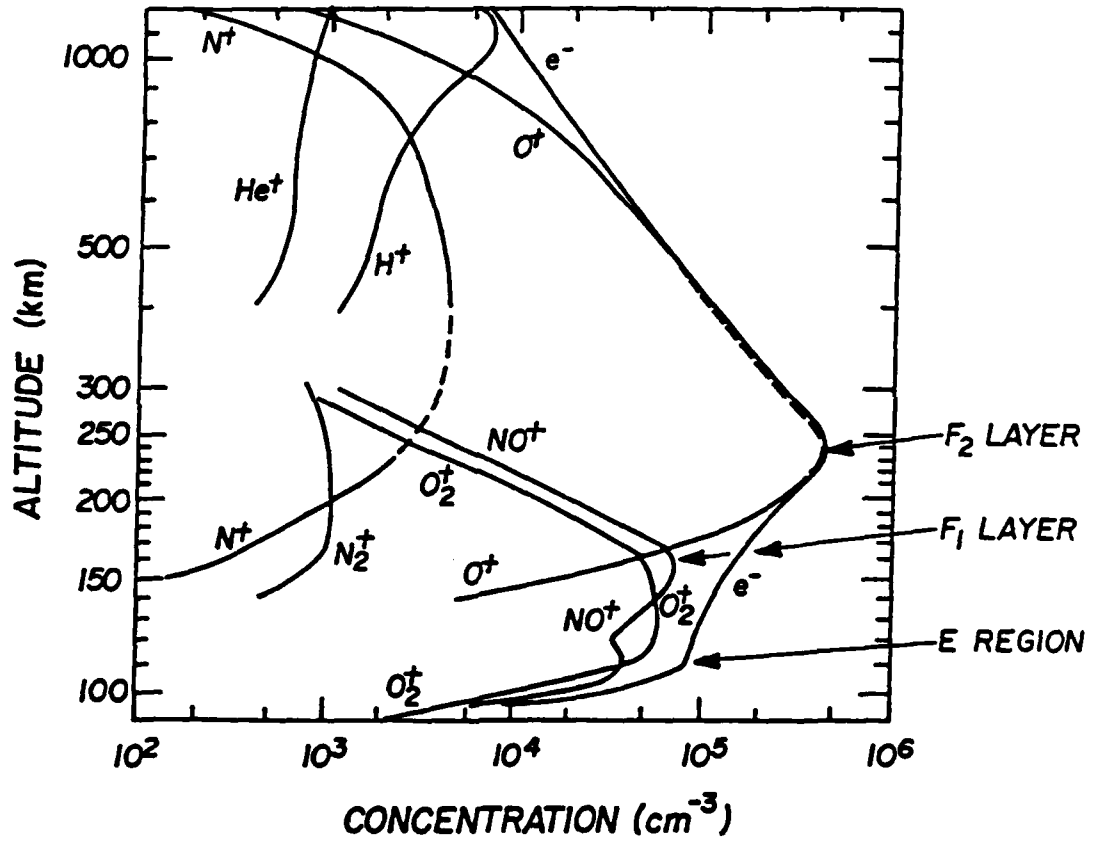

Figure 9. Concentration levels for ions from 90 to 1020 km (D. Torr 1985).

an atom or molecule will resonantly scatter a solar photon of wavelength λ into 4π Sr in unit time," called a g factor according to Donn et al. (1974). The form of g factor used for calculation in this paper is taken from Barth (1965) and is given as follows:

$$g = \pi F_{OV'} (\pi e^2/mc^2) \lambda^2_{OV'} f_{XN} q_{OV'} \tilde{W}_{V'V"}$$

and

$$g'_{V'V"} = g_{V'V"} f_{XN}, \qquad f_{XN} = \frac{f_{OV'}}{q_{OV'}}$$

where F = solar flux, e = electron charge, m = electron mass, c = speed of light, q = Frank-Condon factor, $\tilde{W}$ = albedo for single-scattering of the fluorescent band, V'V" = fluorescent band in emission, OV' absorption band in the lowest vibrational level of the ground electronic state, f = oscillator strength and F_{XN} = the band oscillation strength for the electronic transition from ground state X to excited state N.

Values of g' and q are provided by Barth (1965). Using the formulas discussed above to calculate g:

$$1. \quad g_{V'V"} = \frac{g'_{V'V"} q_{OV'}}{f_{OV'}}$$

Therefore oscillator strengths ($f_{OV'}$) are needed to complete the emission rate factor calculation for each of the carbon oxide UV emission bands.

When the oscillator strength ($f_{OV'}$) was not found in the literature, the Einstein coefficient (A) was used to calculate the oscillator strength. This calculation is very simple and needs to

be done from measurements of transition probabilities, according to Joshi et al. (1966). They found the proper equation to be:

$$f_{0V'} = 1.5 \times 10^{-8} \quad \lambda^2_{V'V''} A_{V'V''}$$

with λ in um and A in sec^{-1} .

Using Equation 1, Tables 3 and 4 show $A_{V'V''}$ if used, $f_{0V'}$, g' and the g factors which were calculated for the CO fourth positive and Cameron bands. Tables 5 and 6 show the constants used to calculate the g factors for the CO^+ comet tail and first negative bands. There are no known ultra-violet emissions by CO_2. For CO_2^+ the author could find only one band system emitted in the ultraviolet, the Fox Duffendack and Barken Bands (Pearse and Gaydon, 1984). However, an extensive literature search failed to find all of the constants necessary to calculate the emission rate factor.

To calculate vertical brightness, the following equation is used (M. Torr, 1985):

$$\text{Brightness} = [X]\ H\ g\ 1.0 \times 10^{-6}\ \text{Rayleighs}$$

with [X] the concentration of CO^+ or CO_2^+, in cm^3sec^{-1}, H the scale height in cm, g = the emission rate factor in photons/sec and the conversion factor from photons/cm^2sec to Rayleighs. Using this equation, the concentration calculations or measurements and the g factor calculation we obtain brightenss values with respect to height. See Table 8 for the CO Cameron and Table 7 for the fourth positive bands brightness predictions. Table 9 provides the brightness calculations for the CO^+ comet tail and Table 10 the first negative bands.

Table 3. g factor calculation for CO Fourth Positive bands.

V'V"	$f_{0V'} \times 10^{-3}$ (Hessen and Dressler, 1965)	q	$g'_{V'V"}$ (photons/sec)	$g_{V'V"}$ (photons/sec)
0 0	9.0	1.13×10^{-1}	5.38×10^{-7}	4.28×10^{-8}
0 1	20.1	2.61×10^{-1}	1.12×10^{-6}	8.63×10^{-8}
0 2	21.2	2.85×10^{-1}	1.1×10^{-6}	8.18×10^{-8}
0 3	14.1	1.96×10^{-1}	6.85×10^{-7}	4.93×10^{-8}
0 4	6.7	9.6×10^{-2}	3.01×10^{-7}	2.1×10^{-8}
0 5	2.4	3.55×10^{-2}	9.97×10^{-8}	6.7×10^{-9}
0 6	20.2	2.16×10^{-1}	2.17×10^{-6}	2.03×10^{-7}
1 1	14.0	1.55×10^{-1}	1.41×10^{-6}	1.3×10^{-7}
1 2	0.3	3.05×10^{-3}	2.51×10^{-8}	2.5×10^{-9}
1 3	6.5	7.64×10^{-2}	5.66×10^{-7}	4.8×10^{-8}
1 4	15.8	1.93×10^{-1}	1.29×10^{-6}	1.1×10^{-7}
1 5	19.7	1.86×10^{-1}	1.11×10^{-6}	1.2×10^{-7}
1 6	8.2	1.08×10^{-1}	5.81×10^{-7}	4.4×10^{-8}
1 7	3.3	4.45×10^{-2}	2.13×10^{-7}	1.6×10^{-8}
2 0	22.6	2.3×10^{-1}	1.9×10^{-6}	1.9×10^{-7}
2 1	1.2	1.22×10^{-2}	9.14×10^{-8}	9.0×10^{-9}
2 2	8.3	9.01×10^{-2}	6.13×10^{-7}	5.7×10^{-8}
2 3	10.3	1.16×10^{-1}	7.14×10^{-7}	6.3×10^{-8}
2 4	0.4	5.08×10^{-3}	2.82×10^{-8}	2.2×10^{-9}
2 5	4.8	5.72×10^{-2}	2.86×10^{-7}	2.4×10^{-8}
2 6	13.2	1.65×10^{-1}	7.41×10^{-7}	5.9×10^{-8}
2 7	12.9	1.67×10^{-1}	6.71×10^{-7}	5.2×10^{-8}
2 8	7.4	9.96×10^{-2}	3.58×10^{-7}	2.7×10^{-8}
2 9	3.0	4.13×10^{-2}	1.32×10^{-7}	9.6×10^{-9}

V' = upper vibrational state

V" = lower vibrational state

Table 4. g factor calculation for CO Cameron bands.

V'V"	$A_{V'V"}$ (sec^{-1}) (James, 1971)	$f_{V'V"}$	q	g' (photon/sec)	g (photon/sec)
0 0	255	1.63×10^{-7}	2.66×10^{-1}	5.72×10^{-4}	3.5×10^{-10}
0 1	272	1.91×10^{-7}	3.78×10^{-1}	7.1×10^{-4}	3.6×10^{-10}
0 2	122	9.43×10^{-8}	2.4×10^{-1}	3.91×10^{-4}	1.5×10^{-10}
0 3	31.2	2.66×10^{-8}	8.95×10^{-2}	1.26×10^{-4}	3.7×10^{-11}
0 4	4.92	4.63×10^{-9}	2.2×10^{-2}	2.67×10^{-5}	5.6×10^{-12}
0 5	0.44	4.6×10^{-10}	3.79×10^{-3}	3.93×10^{-6}	4.8×10^{-13}
0 6	0.03	3.49×10^{-11}	4.68×10^{-4}	4.13×10^{-7}	3.1×10^{-14}
0 7	<0.01	1.3×10^{-11}	4.24×10^{-5}	3.15×10^{-8}	9.7×10^{-15}
1 0	335	1.99×10^{-7}	3.19×10^{-1}	4.91×10^{-4}	3.1×10^{-10}
1 1	11.8	7.722×10^{-9}	2.88×10^{-2}	3.89×10^{-5}	1.0×10^{-11}
1 2	94.1	6.74×10^{-8}	1.03×10^{-1}	1.22×10^{-4}	8.0×10^{-11}
1 3	146	1.15×10^{-7}	2.65×10^{-1}	2.72×10^{-4}	1.2×10^{-10}
1 4	67.5	5.84×10^{-8}	1.92×10^{-1}	1.7×10^{-4}	5.2×10^{-11}
1 5	15.4	1.47×10^{-8}	7.24×10^{-2}	5.53×10^{-5}	1.1×10^{-11}
1 6	2.16	2.3×10^{-9}	1.71×10^{-2}	1.12×10^{-5}	1.5×10^{-12}
1 7	0.19	2.25×10^{-10}	2.72×10^{-3}	1.51×10^{-6}	1.2×10^{-13}
1 8	0.03	3.97×10^{-11}	3.04×10^{-4}	1.43×10^{-7}	1.9×10^{-14}
1 9	<0.01	1.49×10^{-11}	2.43×10^{-5}	9.59×10^{-9}	5.9×10^{-15}

Table 5. g factor calculation for CO^+ Comet Tail bands.

V'V"	$f_{V'V"}$ (Jain and Sahni, 1966)	q	g' (photon/sec)	g (photon/sec)
0 0	1.56×10^{-4}	4.2×10^{-2}	4.82×10^{-2}	1.8×10^{-4}
0 1	4.34×10^{-4}	1.49×10^{-1}	1.22×10^{-1}	3.6×10^{-4}
0 2	4.56×10^{-4}	2.46×10^{-1}	1.38×10^{-1}	2.6×10^{-4}
0 3	2.07×10^{-4}	2.49×10^{-1}	9.11×10^{-2}	8.0×10^{-5}
0 4	2.45×10^{-5}	1.74×10^{-1}	3.91×10^{-2}	5.5×10^{-6}
0 5	4.55×10^{-5}	1.13×10^{-1}	3.46×10^{-1}	1.4×10^{-3}
1 1	6.73×10^{-4}	1.91×10^{-1}	4.27×10^{-1}	1.5×10^{-3}
1 2	2.15×10^{-4}	8.3×10^{-2}	1.31×10^{-1}	3.4×10^{-4}
1 3	2.38×10^{-7}	0	0	0
1 4	4.89×10^{-5}	8.4×10^{-2}	5.84×10^{-2}	3.4×10^{-5}
1 5	7.8×10^{-6}	1.83×10^{-1}	7.7×10^{-2}	3.3×10^{-6}
2 0	6.84×10^{-4}	1.66×10^{-1}	5.83×10^{-1}	2.4×10^{-3}
2 1	3.85×10^{-4}	9.9×10^{-2}	2.59×10^{-1}	1.0×10^{-3}
2 2	8.26×10^{-6}	2.0×10^{-3}	3.8×10^{-3}	1.7×10^{-5}
2 3	2.44×10^{-4}	1.04×10^{-1}	1.39×10^{-1}	3.3×10^{-4}
2 4	1.11×10^{-4}	8.9×10^{-2}	8.01×10^{-2}	8.5×10^{-5}
2 5	6.84×10^{-7}	10.0×10^{-4}	5.76×10^{-4}	3.9×10^{-7}
3 0	7.05×10^{-4}	1.8×10^{-1}	5.72×10^{-1}	2.2×10^{-3}
3 1	5.64×10^{-5}	1.5×10^{-2}	3.62×10^{-2}	1.4×10^{-4}
3 2	2.72×10^{-4}	7.1×10^{-2}	1.27×10^{-1}	4.9×10^{-4}
3 3	2.13×10^{-4}	7.2×10^{-2}	9.31×10^{-2}	2.8×10^{-4}
3 4	5.46×10^{-6}	2.0×10^{-3}	1.8×10^{-3}	4.9×10^{-6}
4 0	5.59×10^{-4}	1.59×10^{-1}	3.5×10^{-1}	1.2×10^{-3}
4 1	1.93×10^{-5}	4.0×10^{-3}	6.8×10^{-3}	3.3×10^{-5}
4 2	3.87×10^{-4}	9.6×10^{-2}	1.23×10^{-1}	5.0×10^{-4}
4 3	3.55×10^{-6}	10.0×10^{-4}	9.49×10^{-4}	3.4×10^{-6}

Table 6. g factor calculation for CO^+ First Negative bands.

V'V"	$f_{V'V"}$ (Joshi et al. (1966)	q	g' (photon/sec)	g (photon/sec)
0 0	0.0088	5.31×10^{-1}	7.84×10^{-3}	1.2×10^{-4}
0 1	0.0062	3.39×10^{-1}	4.32×10^{-3}	8×10^{-5}
0 2	0.0021	1.04×10^{-1}	1.14×10^{-3}	2.3×10^{-5}
0 3	0.0005	2.14×10^{-2}	2.0×10^{-4}	4.7×10^{-6}
0 4	0.0001	3.38×10^{-3}	2.68×10^{-5}	7.9×10^{-7}
1 0	0.0048	3.13×10^{-1}	2.0×10^{-3}	3.1×10^{-5}
1 1	0.0010	5.65×10^{-2}	3.14×10^{-4}	5.6×10^{-6}
1 2	0.0054	3.18×10^{-1}	1.53×10^{-3}	2.8×10^{-5}
1 3	0.0045	2.17×10^{-1}	8.95×10^{-4}	1.8×10^{-5}
1 4	0.0017	7.49×10^{-2}	2.6×10^{-4}	5.9×10^{-6}
2 0	0.0016	1.11×10^{-1}	1.16×10^{-4}	1.7×10^{-6}
2 1	0.0041	2.58×10^{-1}	2.33×10^{-4}	3.7×10^{-6}
2 2	0.0003	1.76×10^{-2}	1.39×10^{-5}	2.4×10^{-7}
2 3	0.0028	1.46×10^{-1}	9.94×10^{-5}	1.9×10^{-6}
2 4	0.0055	2.55×10^{-1}	1.49×10^{-4}	3.2×10^{-6}

Table 7. Brightness (R) calculations for CO Fourth Positive bands.

V'V"	Height (kM) 70	75	80	85	90	95	100
0 0	89	50	24	15	13	13	7
0 1	178	101	49	30	27	27	14
0 2	169	96	46	28	25	25	13
0 3	102	58	28	17	15	15	9
0 4	43	25	12	7	7	7	3
0 5	14	8	4	2	2	2	1
1 0	420	238	115	70	63	63	32
1 1	269	153	74	45	40	40	21
1 2	5	3	1	0.9	0.8	0.8	0.4
1 3	99	56	27	17	15	15	8
1 4	228	129	62	38	34	34	18
1 5	248	141	68	41	37	37	19
1 6	91	52	25	15	14	14	7
1 7	33	19	9	6	5	5	3
2 0	393	223	108	66	59	59	30
2 1	19	11	5	3	3	3	1
2 2	118	67	32	20	18	18	9
2 3	130	74	36	22	20	20	10
2 4	5	3	1	0.8	0.7	0.7	0.4
2 5	50	28	14	8	8	8	4
2 6	122	69	33	20	18	18	9
2 7	108	61	29	18	16	16	8
2 8	56	32	15	9	8	8	4
2 9	20	11	5	5	3	3	1

Table 8. Brightness (R) calculations for CO Cameron bnads.

V'V"	Height (km) 70	75	80	85	90	95	100
0 0	0.7	0.4	0.2	0.1	0.1	0.1	0.06
0 1	0.8	0.4	0.2	0.1	0.1	0.1	0.06
0 2	0.3	0.2	0.9	0.05	0.05	0.05	0.02
0 3	0.08	0.04	0.02	0.01	0.01	0.01	0.006
0 4	0.01	0.007	0.003	0.002	0.002	0.002	0.0009
0 5	0.00099	5×10^{-4}	3×10^{-4}	1.6×10^{-4}	1.5×10^{-4}	1.5×10^{-4}	7.6×10^{-5}
0 6	6.4×10^{-5}	3.6×10^{-5}	1.8×10^{-5}	1.1×10^{-5}	1.1×10^{-5}	1.1×10^{-5}	5×10^{-6}
0 7	2×10^{-5}	1.1×10^{-5}	6×10^{-6}	3×10^{-6}	3×10^{-6}	3×10^{-6}	1.5×10^{-6}
1 0	0.6	0.4	0.2	0.1	0.1	0.1	0.05
1 1	0.02	0.01	6×10^{-3}	3×10^{-3}	3×10^{-3}	3×10^{-3}	2×10^{-3}
1 2	0.2	0.09	0.05	0.03	0.03	0.03	0.01
1 3	0.3	0.1	0.07	0.04	0.04	0.04	0.02
1 4	0.1	0.06	0.03	0.02	0.02	0.02	8×10^{-3}
1 5	0.002	0.01	6×10^{-3}	4×10^{-3}	3×10^{-3}	3×10^{-3}	2×10^{-3}

Table 8. Continued

V'V"	Height (km) 70	75	80	85	90	95	100
1 6	3×10^{-3}	2×10^{-3}	9×10^{-4}	5×10^{-4}	5×10^{-4}	$5\times1-^{-4}$	2×10^{-4}
1 7	3×10^{-4}	7×10^{-4}	4×10^{-5}	4×10^{-5}	4×10^{-4}	4×10^{-4}	2×10^{-5}
1 8	4×10^{-5}	2×10^{-5}	1×10^{-5}	7×10^{-6}	6×10^{-6}	6×10^{-6}	3×10^{-6}
1 9	1×10^{-5}	7×10^{-6}	3×10^{-6}	2×10^{-6}	2×10^{-6}	2×10^{-6}	9×10^{-7}

Table 9. Brightness (R) calculations for CO^+ Comet Tail bands.

	Height (km)						
V'V"	70	75	80	85	90	95	100
0 0	1.3×10^{-4}	--	--	--	--	--	--
0 1	2.5×10^{-4}	--	--	--	--	--	--
0 2	1.8×10^{-4}	--	--	--	--	--	--
0 3	5.6×10^{-5}	--	--	--	--	--	--
0 4	3.9×10^{-6}	--	--	--	--	--	--
1 0	9.8×10^{-4}	--	--	--	--	--	--
1 1	1.1×10^{-3}	--	--	--	--	--	--
1 2	2.4×10^{-4}	--	--	--	--	--	--
1 3	0	--	--	--	--	--	--
1 4	2.4×10^{-5}	--	--	--	--	--	--
1 5	2.3×10^{-6}	--	--	--	--	--	--
2 0	1.7×10^{-3}	--	--	--	--	--	--
2 1	7×10^{-4}	--	--	--	--	--	--
2 2	1.2×10^{-5}	--	--	--	--	--	--
2 3	2.3×10^{-4}	--	--	--	--	--	--
2 4	6×10^{-6}	--	--	--	--	--	--
2 5	2.7×10^{-7}	--	--	--	--	--	--
3 0	1.5×10^{-3}	--	--	--	--	--	--
3 1	1×10^{-4}	--	--	--	--	--	--
3 2	3.4×10^{-4}	--	--	--	--	--	--
3 3	2×10^{-4}	--	--	--	--	--	--
3 4	3×10^{-6}	--	--	--	--	--	--
4 0	8×10^{-4}	--	--	--	--	--	--
4 1	2.3×10^{-5}	--	--	--	--	--	--
4 2	3.5×10^{-4}	--	--	--	--	--	--
4 3	2.4×10^{-6}	--	--	--	--	--	--

-- Value <<<0.0

Table 10. Brightness (R) calculations for CO^+ First Negative bands.

	Height (km)						
V'V"	70	75	80	85	90	95	100
0 0	8.4×10^{-5}	--	--	--	--	--	--
0 1	5.6×10^{-5}	--	--	--	--	--	--
0 2	1.6×10^{-5}	--	--	--	--	--	--
0 3	3.3×10^{-6}	--	--	--	--	--	--
0 4	5.5×10^{-7}	--	--	--	--	--	--
1 0	2.2×10^{-5}	--	--	--	--	--	--
1 1	3.9×10^{-6}	--	--	--	--	--	--
1 2	2×10^{-5}	--	--	--	--	--	--
1 3	1.3×10^{-5}	--	--	--	--	--	--
1 4	4.1×10^{-6}	--	--	--	--	--	--
2 0	1.2×10^{-6}	--	--	--	--	--	--
2 1	2.6×10^{-6}	--	--	--	--	--	--
2 2	1.7×10^{-7}	--	--	--	--	--	--
2 3	1.3×10^{-6}	--	--	--	--	--	--
2 4	2.2×10^{-6}	--	--	--	--	--	--

-- Values <<<0.0

The theoretical brightness calculations indicate that neither of the CO^+ bands will be observable by the ISO. For the CO bands the best possibility for ISO appears to be the fourth positive bands. However, there could be errors in the photochemical theory and underlying assumptions. It is therefore, wise to investigate the data provided from the ISO to see if all or any of the mentioned bands were actually observed.

RESULTS

The results from analyzing the data measured by the ISO are presented below. This includes data containing mesospheric dayglow and the shuttle induced vehicle glow. The technique used to analyze both sets of data are similar.

Dayglow

To determine if the ISO is observing carbon oxide emission lines in the dayglow, several checks need to be performed. First, all of the carbon oxide lines which appear to be present in the data are located. Because more than one molecule can emit radiation in the same wavelength, it is important to check for other molecules which could fluoresce or resonantly scatter in this same wavelength. If this occurs, then the contribution from each molecule to this line must be determined. After carbon oxide emission lines are selected for study, they must be compared to lines which are better understood. This comparison of intensity verses height will show if the carbon oxide emission lines are actually carbon oxide lines or some other molecule undergoing resonance fluoresence.

The brighteness predictions discussed previously indicate that the CO fourth positive band is the most likely band the ISO could observe. The other band intensities are not bright enough to overcome the ISO's signal threshold or sky background. A signal intensity of approximately 30 R/Å is needed in order for the feature to be observable by the ISO (Torr, Basedow, Torr, 1982)

in an integration period of a few seconds. Therefore, only the CO fourth positive bands will be considered when analyzing the mesospheric dayglow data.

Due to a spurious feature, possibly scattered sunlight, in all but two of the spectra measured by the ISO, the mesospheric dayglow data is very limited. This light leak occurred in the same wavelength region where the CO fourth positive bands should be their brightest (1478 Å to 1800 Å). The intensity of the unexplained feature was strong enough to completely dominate any CO fourth positive emission lines in this region. Another difficulty occurred when one of the five spectrometers (near UV) suffered from impaired gain due to damage incurred during integration to the shuttle. The spectrometer in question covered the wavelengths from 2200 Å to 4100 Å (Torr, Basedow, Torr, 1982). The resulting spectrum was not obtained with sufficient sensitivity for this study. Most of the other carbon oxide bands (CO^+ first negative, CO cameron, CO^+ comet tail, etc.) emit within this region.

These data restrictions eliminate all but two spectra which contain mesospheric carbon oxide UV emissions. Realizing that this is a very limited data base, it is thought that averaging the two spectra together will create a better representation of mesospheric dayglow. This spectrum is shown in Figure 10.

Any CO fourth positive lines which appeared on the averaged spectrum were located and noted (Fig. 10). This was done using the spectrum produced by the synthetic spectral model. All of the observable lines occur in the one through three upper vibrational levels.

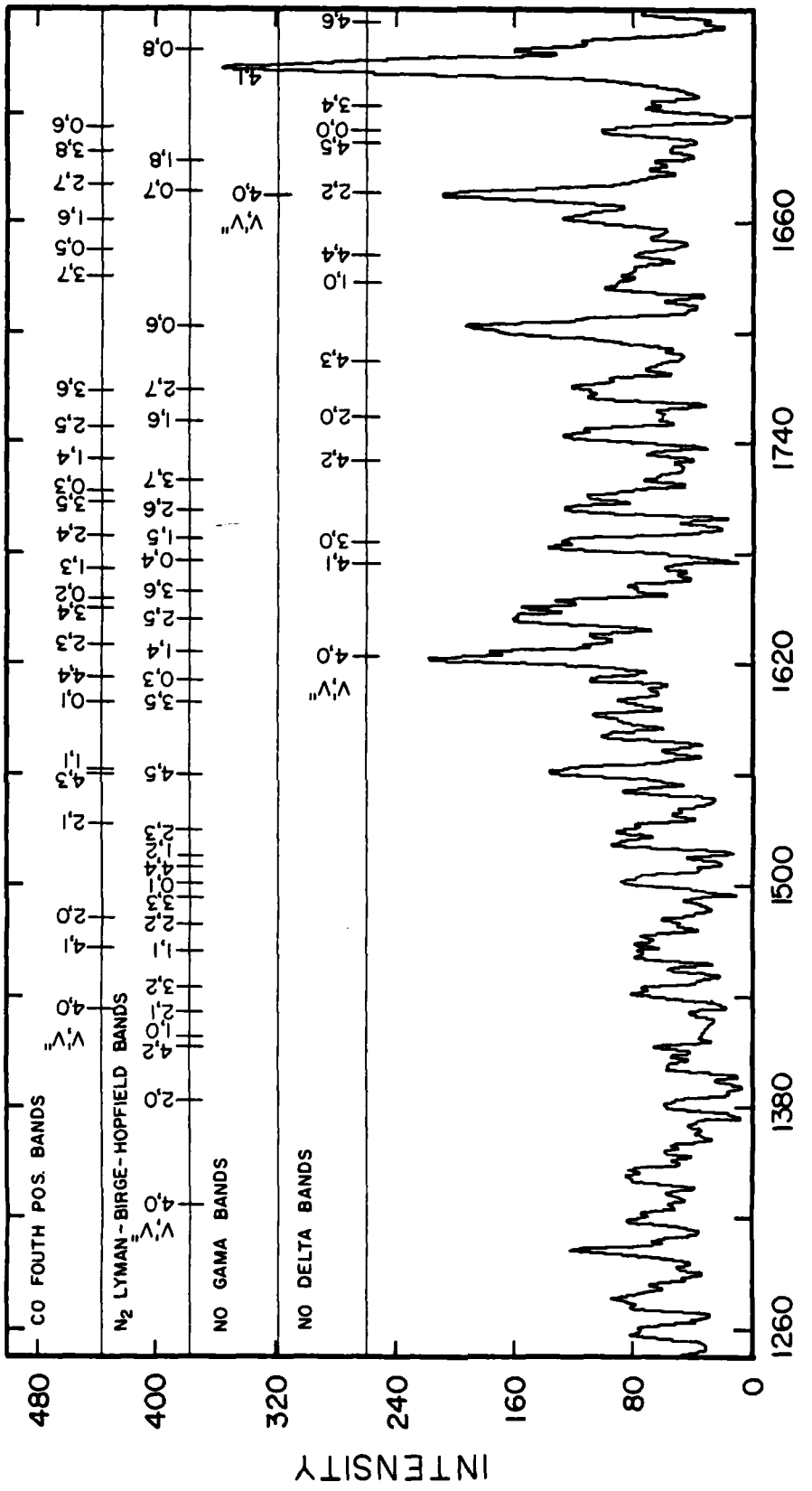

Fig. 10. Averaged mesospheric dayglow spectra.

However, there are several other molecules which emit in this wavelength region. These include the NO delta, NO gamma and the N_2 Lyman-Birge-Hopfield (LBH) Bands. Any lines from these molecules which appear on the spectrum have been noted on Fig. 10. Many of the N_2 LBH lines are very close to or coincide with the CO fourth positive lines. This occurs because the molecular structure and weight for N_2 is equal to that of CO's causing both molecules to fluoresce and resonantly scatter at approximately the same wavelengths.

When both molecules emit at the same wavelength, it is important to determine how much energy is contributed by each molecule. This allows an estimate of how strongly a line represents a specific molecular band emission (in this case CO fourth positive). In order to do this for a specific molecule, a comparison of relative intensities between lines in the same vibration state but different rotational states must be drawn. As an example, consider the 3,5 CO fourth positive, or as seen on Fig. 10, the 2,6 N_2 LBH line. The line considered for comparison for the 3,5 CO fourth positive line is the 3,8 CO fourth positive line and for the 2,6 N_2 LBH line, a comparison is drawn with the 2,5 LBH line.

A good approximation for determining the energy contribution to this line (3,5 CO or 2,6 N_2) from each molecule is calculated in the following manner. By comparing the Frank-Condon factors of the two lines at the same vibrational level a ratio of their respective intensity levels is known. The Frank-Condon factor is the probability that a molecule will transition from one excited

level to another. Comparing the Frank-Condon factors for the 3,5 CO fourth positive lines, the ratio is shown to be:

$$\frac{\text{3,5 CO fourth positive Frank-Condon factor}}{\text{3,8 CO fourth positive Frnak-Condon factor}} = 0.5$$

This indicates that the 3,5 line should be half as bright as the 3,8 line. For the N_2 LBH lines the ratio is as follows:

$$\frac{\text{2,6 } N_2 \text{ LBH Frank-Condon factor}}{\text{2,5 } N_2 \text{ LBH Frank-Condon factor}} = 76$$

Therefore, the 2,6 line should be approximately seventy-six times brighter than the 2,5 N_2 LBH line.

Looking at Figure 10, it is apparent that only about 10 R/Å of the 2,6 N_2 LBH line is due to the 3,5 CO fourth positive emission. This is because one half of the 3,8 CO fourth positive line is only about 10 R/Å. The N_2 LBH ratio indicates the line should be much larger than the emission intensity actually is. Therefore, this line is mainly caused by the 2,6 N_2 LBH line. This eliminates the 3,5 CO fourth positive line for further consideration.

This process was performed on any jointly shared lines between CO fourth positive and the NO delta, NO gamma and N_2 LBH lines. After this exercise, only three CO fourth positive bands were considered for further study. These lines are the CO fourth positive, 1,6 line, 3,8 and 0,6 line. As shown by Figure 10, there are no other molecular emission lines near these features, thus making them excellent candidates for continued study.

To be sure these three lines are CO and not some other

constituent, an intensity profile must be examined. The two spectra that were used for this were broken into their eight height lines. These lines and respective heights are given in Figures 11 through 18 for the first spectrum considered and Figures 19 through 26 for the second spectrum. The four lines that are considered are noted on all of these figures. The comparison of CO will be done with the NO gamma, 4,0 line. The intensities found for the NO gamma band are similar to that used in determining intensities for the CO fourth positive bands. These line by line spectra will be used to develop an intensity height profile. As stated before, this will permit a comparison with Lippens et al. (1984).

By number integration, the area under each line can be calculated. This results in intensity values for each of the CO fourth positive lines and the NO gamma line. Figure 27 shows the height verses averaged intensity profiles for the first spectrum which varies in altitude from 88 to 102 km. The averaged intensity height profiles for the second spectrum (Fig. 28) varies in height from 98 to 112 km. The CO lines in both figures display an altitude profile similar to that for the NO line. Therefore, it is necessary to compare the ISO's meospheric CO measurements to that of Lippens et al. (1984).

This approach is best to determine if the ISO is observing mesospheric CO. Figure 29 shows Lippens et al. data and the values used for comparison in this paper. Realizing that Lippens data is the vertical height profile and that the data used in this

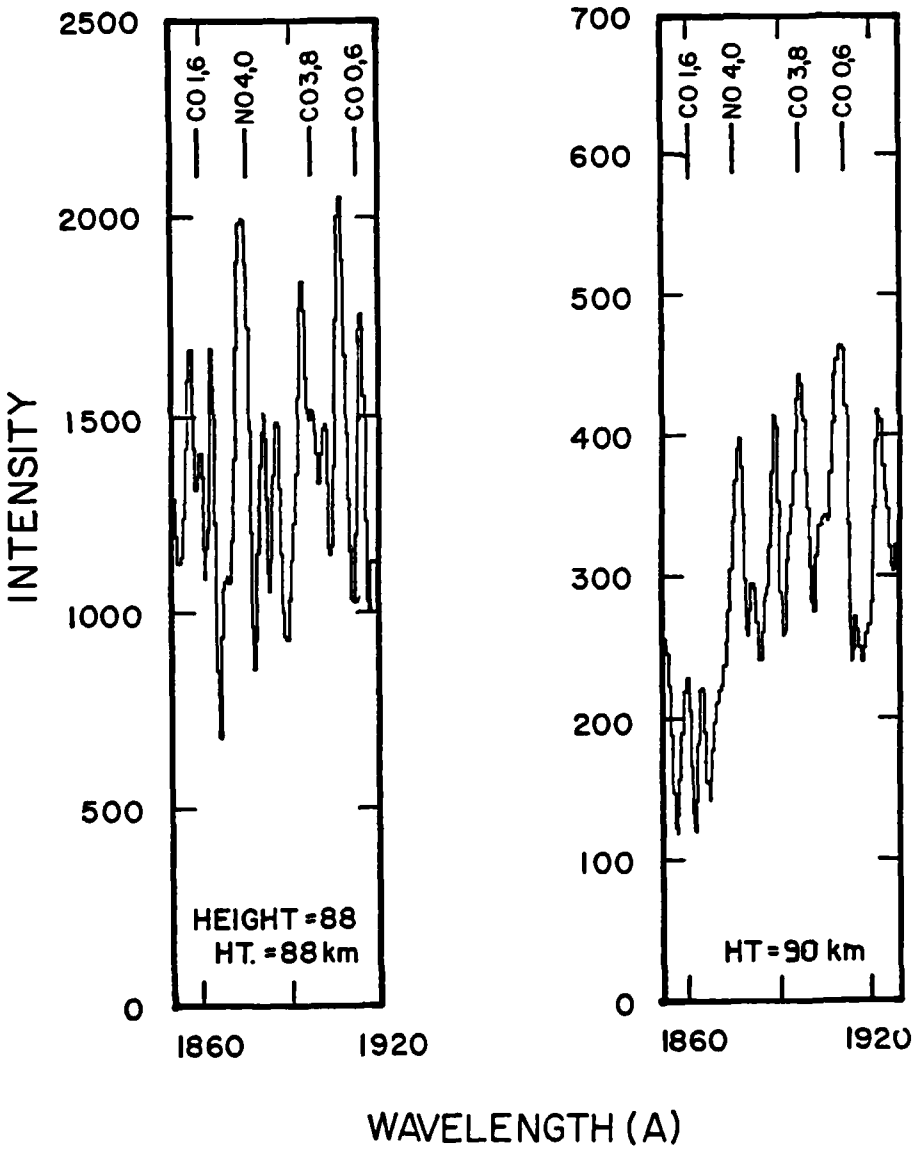

Fig. 11 and Fig. 12. Height profile representation of first spectra.

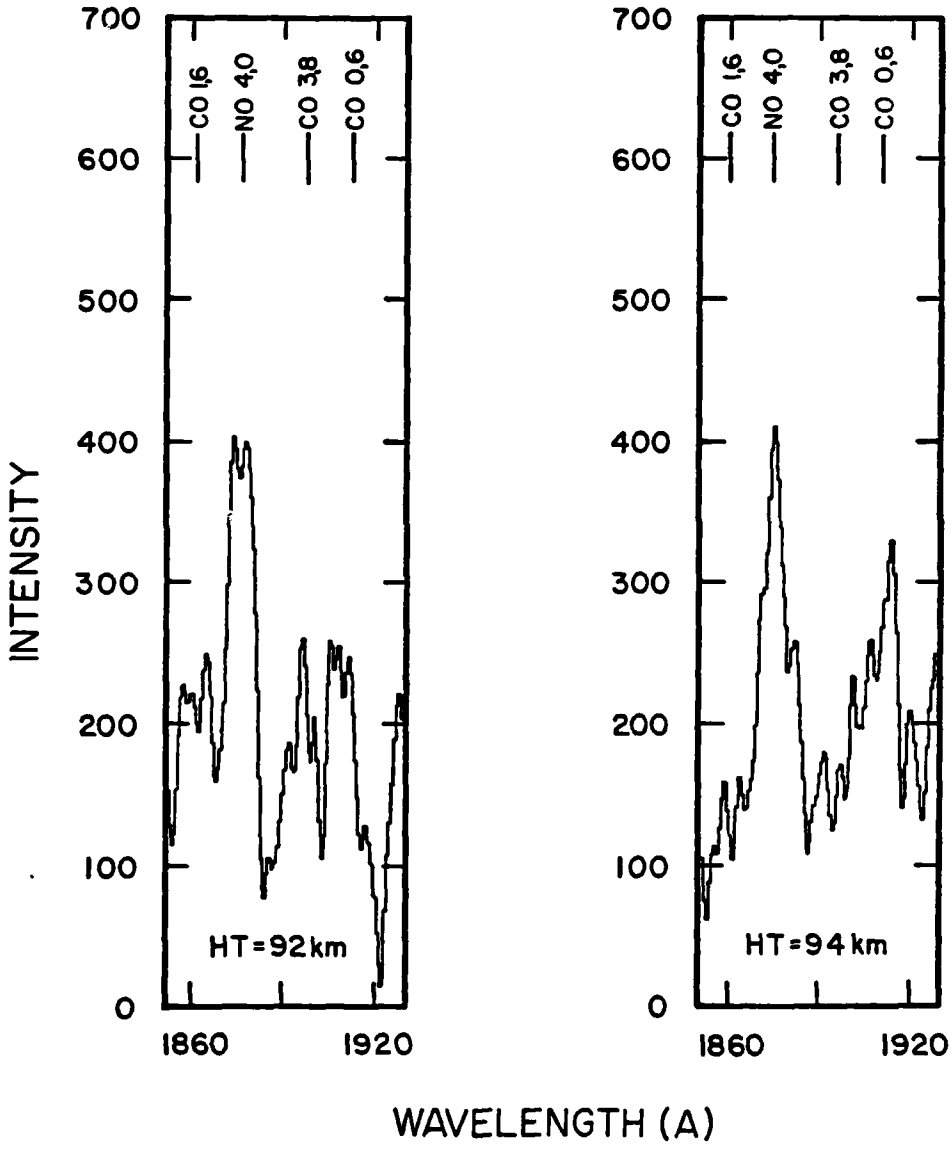

Fig. 13 and Fig. 14. Height profile representation of first spectra.

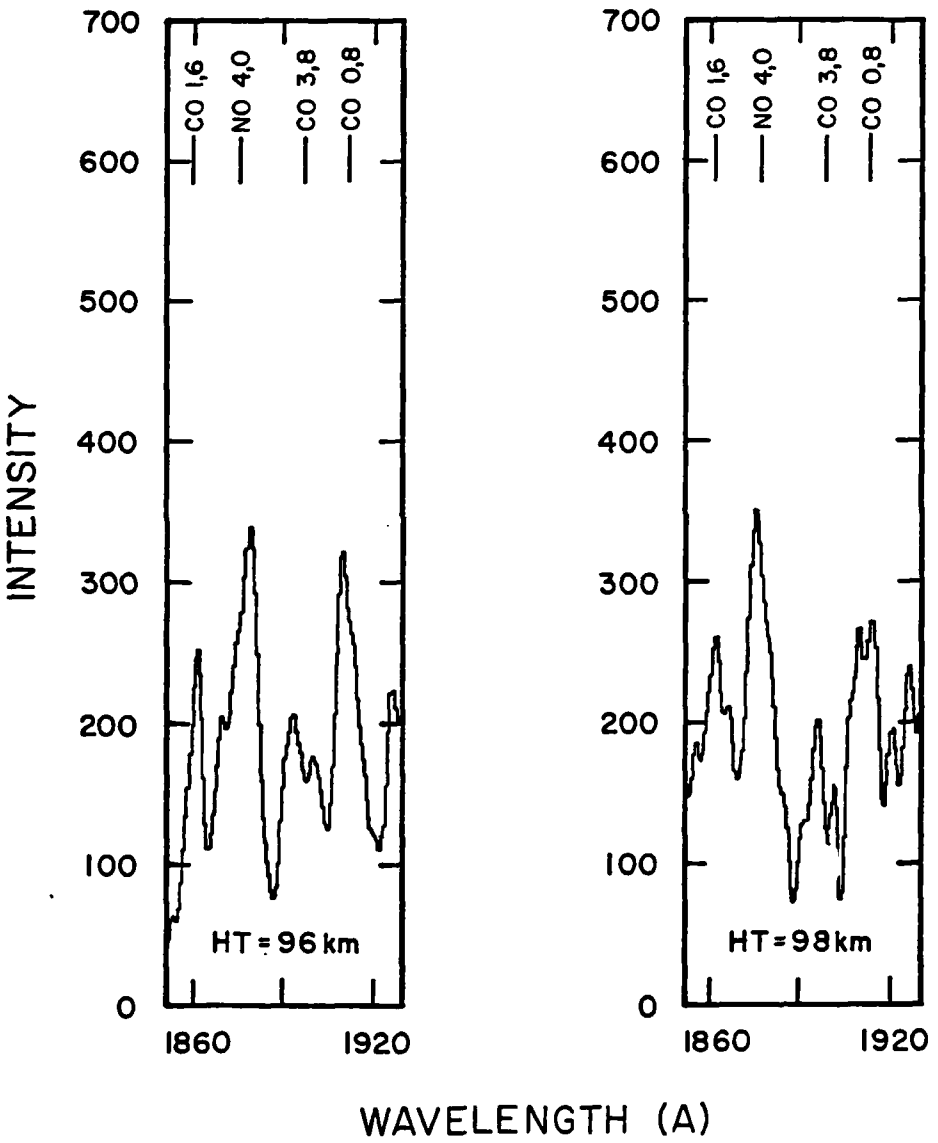

Fig. 15 and Fig. 16. Height profile representation of first spectra.

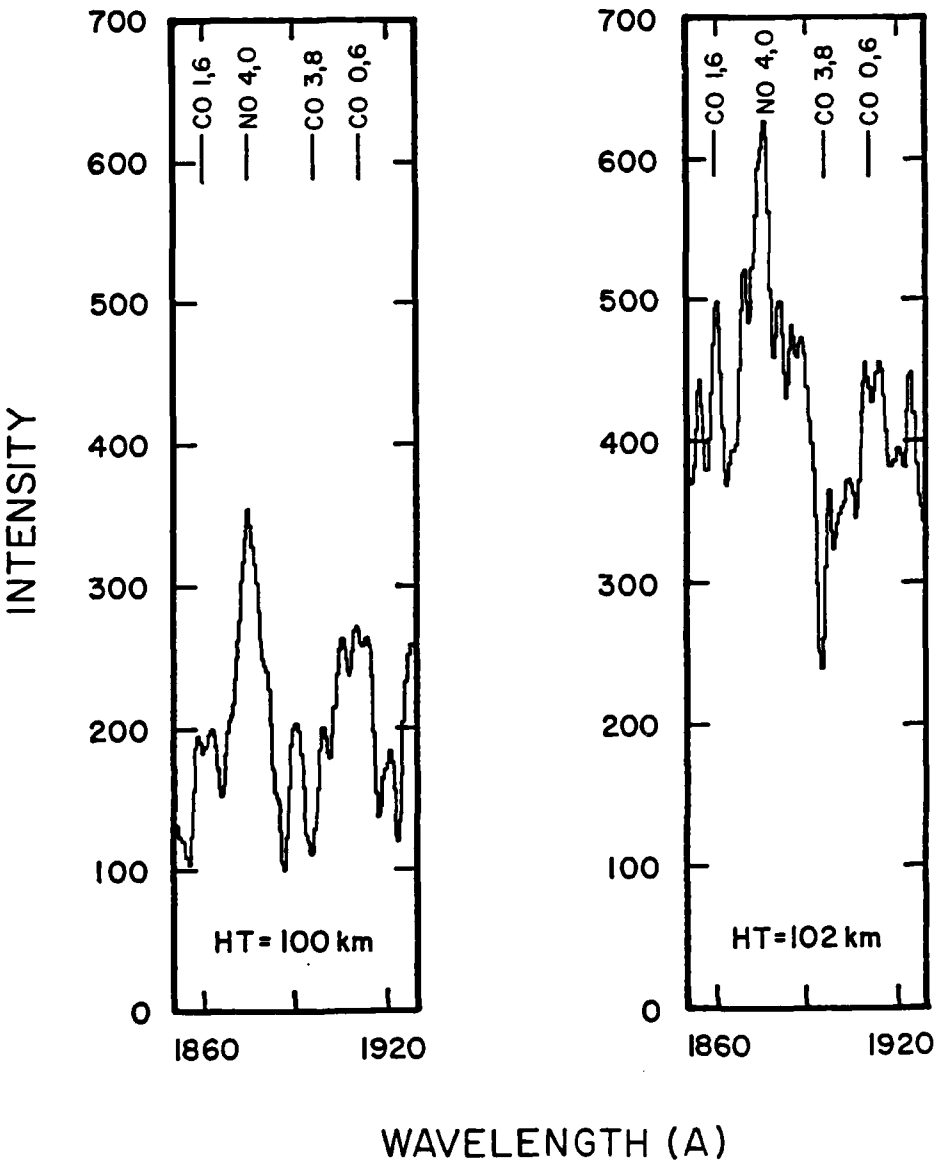

Fig. 17 and Fig. 18. Height profile representation of first spectra.

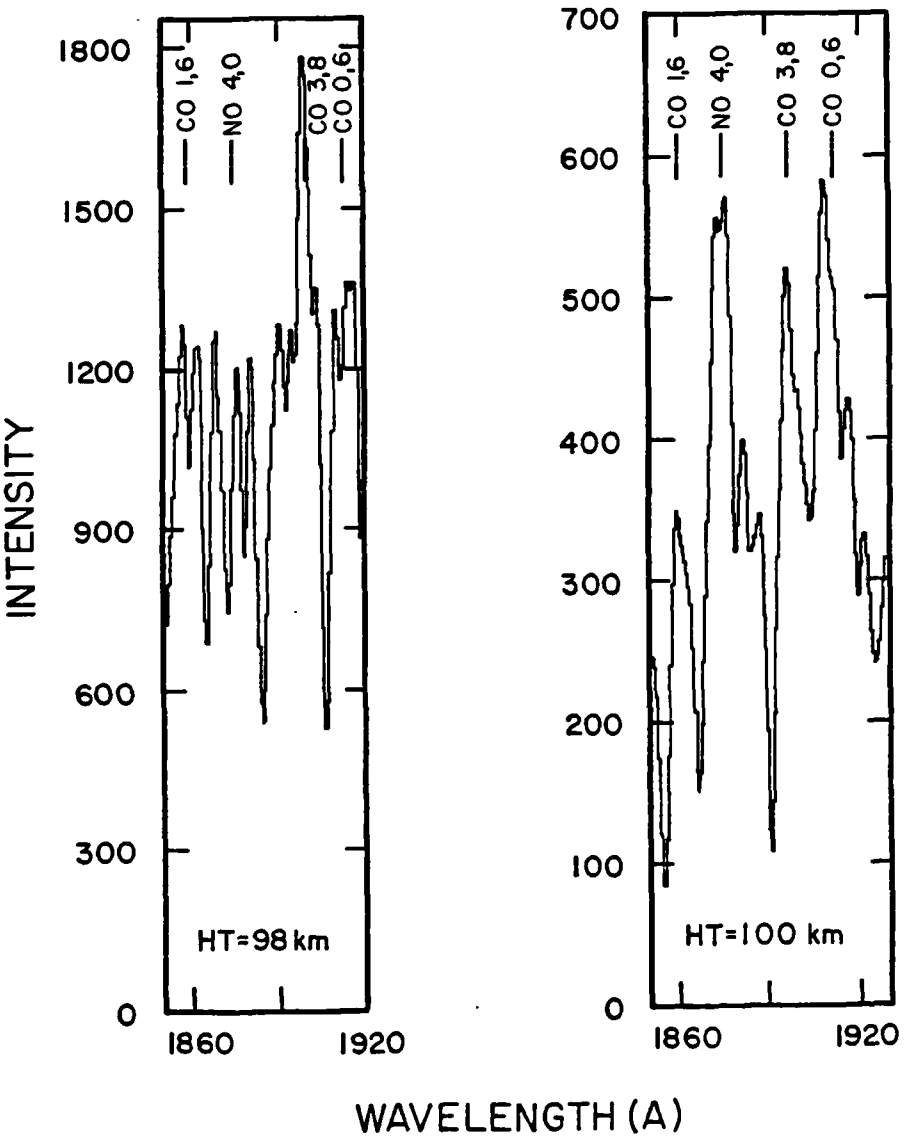

Fig. 19 and Fig. 20. Height profile representation of second spectra.

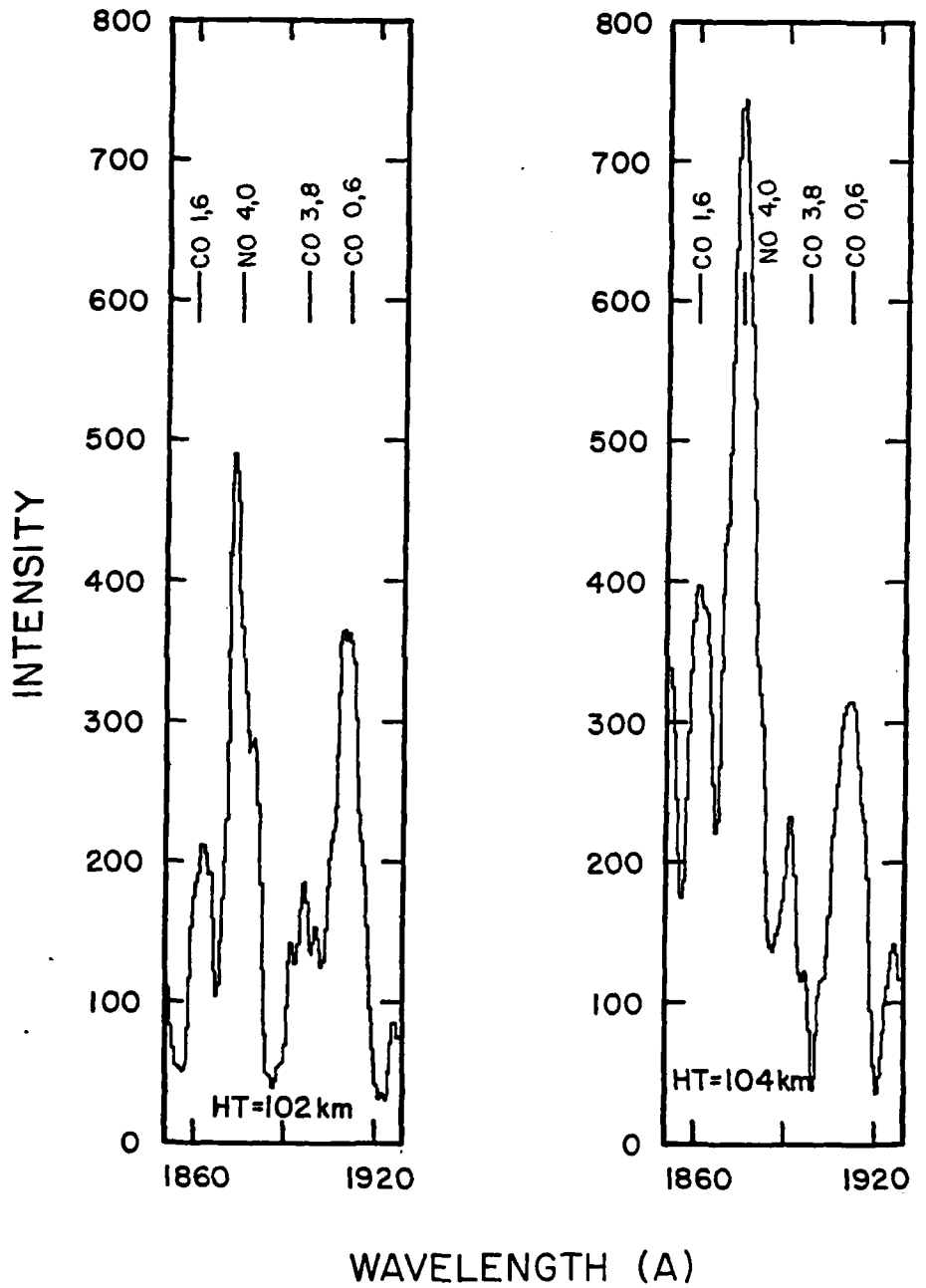

Fig. 21 and Fig. 22. Height profile representation of second spectra.

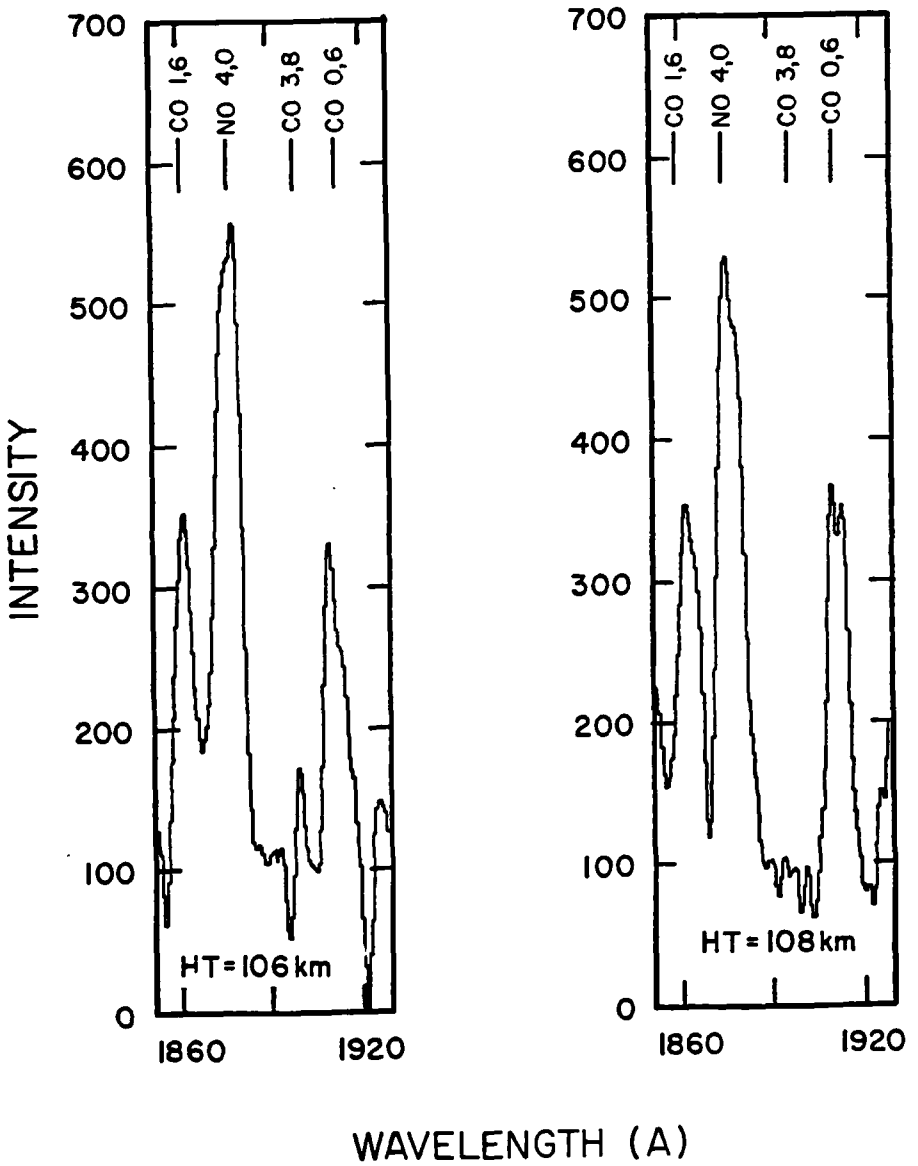

Fig. 23 and Fig. 24. Height profile representation of second spectra.

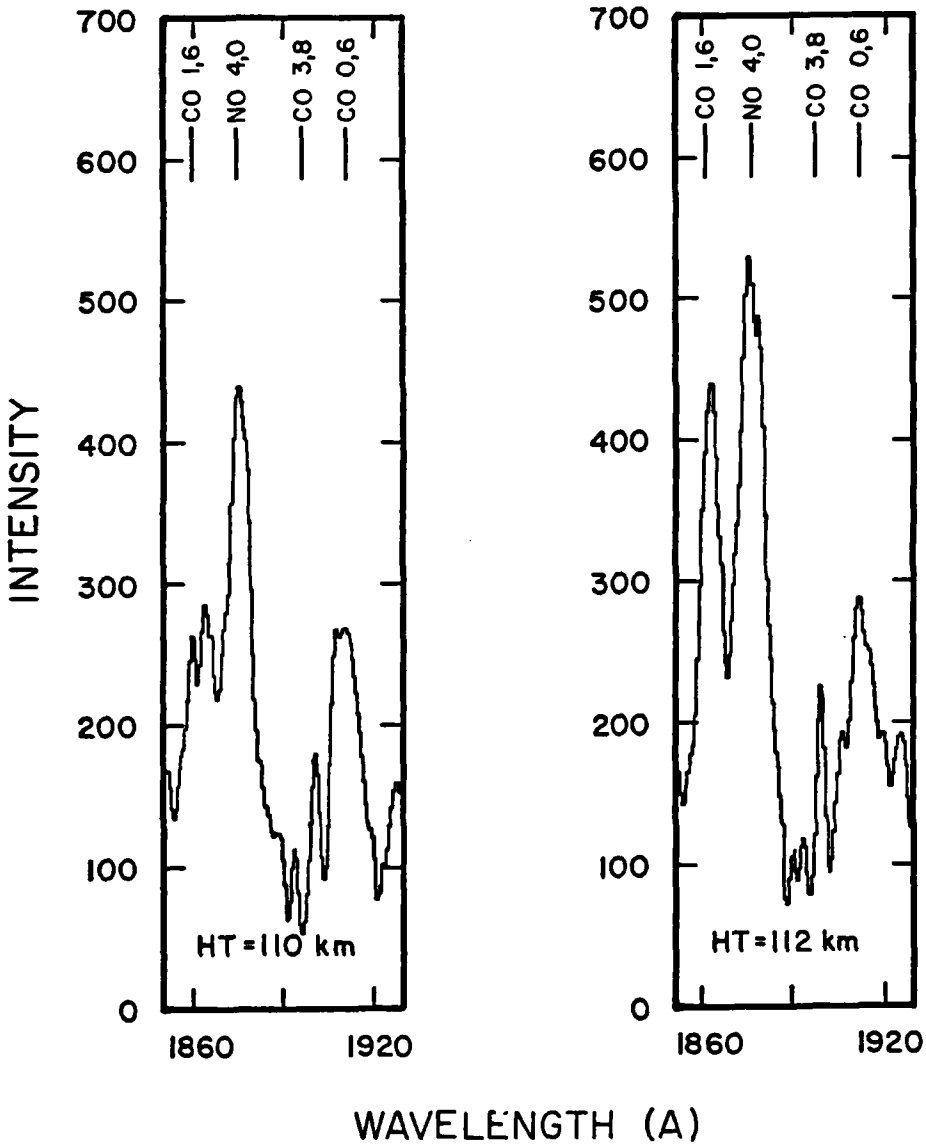

Fig. 25 and Fig. 26. Height profile representation of second spectra.

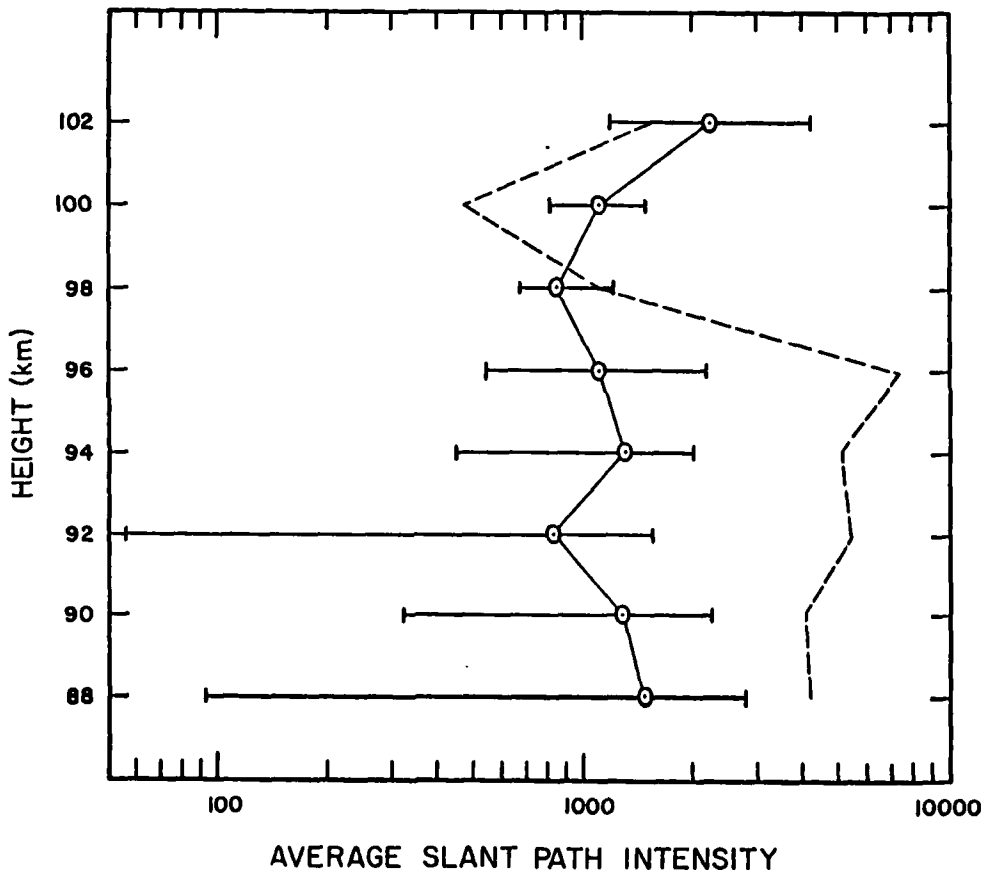

Fig. 27. Average slant path intensity (R) for 88 km to 102 km. Where --- is the NO gamma 4-0 line, 0 is the average intensity of the CO 106, 308 and 0-6 line, and 1--1 represents the maximum and minimum intensity values of the three CO fourth positive bands.

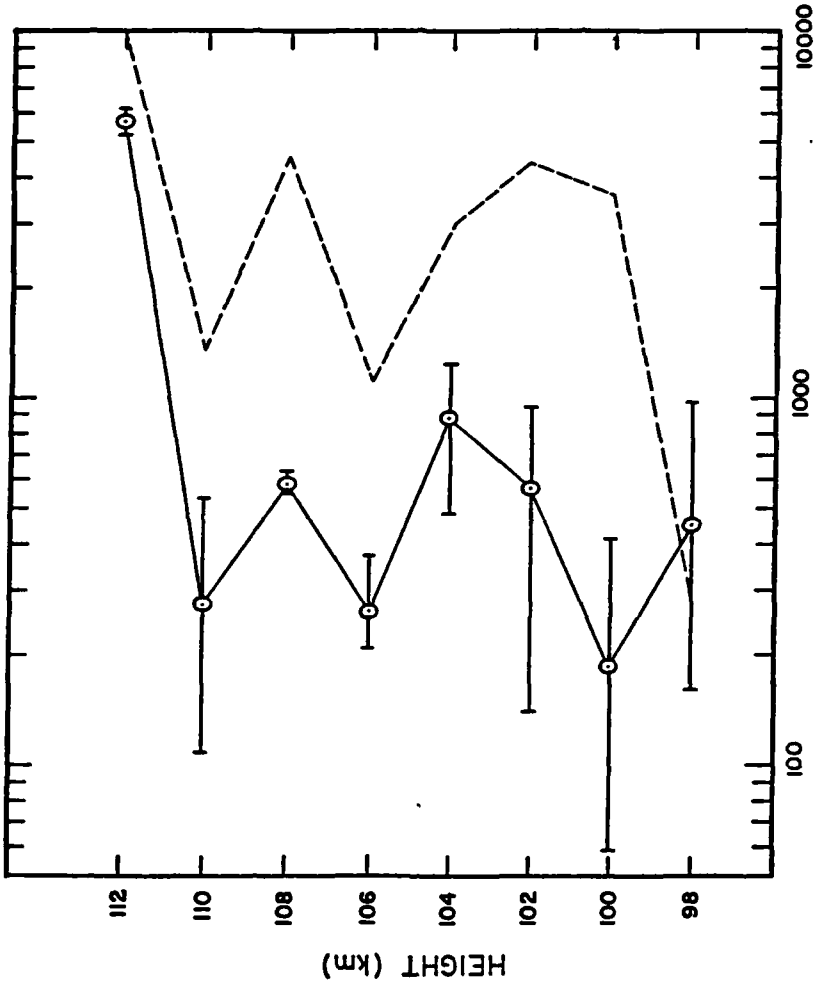

Fig. 28. Average slant path intensity (R) for 98 km to 11.2 km. Where --- is the NO gamma 4-0 line, θ is the average intensity of the CO 106, 3-8 and 0-6 lines, and 1--1 represents the maximum and minimum intensity values of the three CO fourth positive bands.

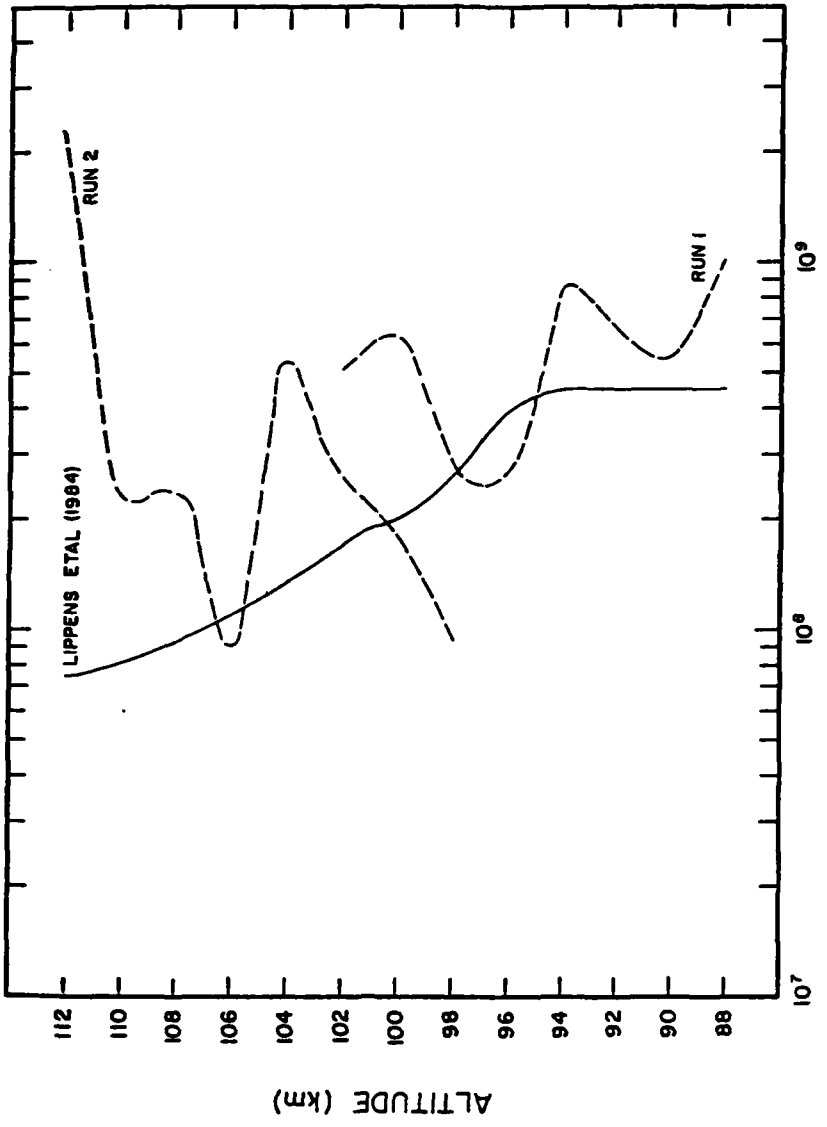

Fig. 29. This is a comparison of CO density height profiles measured in the infrared—(Lippens et al., 1984) to data measured by the ISO in the ultraviolet---$_{\cdot,\mathrm{Run}}$] (88 km to 102 km). Run 2 (98 km to 112 km).

paper is slant path values, it is necessary to convert the ISO's data to vertical height-density values. According to M. Torr (1985) this is done by the following:

$$I_{sl} = \eta H \sqrt{2\pi H}$$

$$\eta = g\,[CO]$$

where I_{sl} is the slant path measured intensity, η is the volume emission rate which is equal to the g factor (g) times the concentration of CO ([CO]), H is the scale height (6.9 km) and $\sqrt{2\pi H}$ is the geometrical correction for the ratios of slant path intensities to vertical intensities. Through substitution for η and algebraic manipulation, the vertical concentration of CO is calculated by:

$$[CO] = \frac{I_{sl}\,(1 + 10^6)\,\text{photons raleigh}}{gH\sqrt{2\pi H} \qquad \text{cm}^2\text{sec}}$$

Table 11 contains the I_{sl} values for the CO 1-6 fourth positive band and calculated vertical density profiles. Figure 30 shows a density versus height plot for both Lippens et al. data and the data as measured by the ISO. It is readily apparent that the ISO is measuring carbon monoxide in the mesosphere.

Shuttle Induced Glow

The process for examining the night ISO data is similar to that used in the analysis of the mesospheric dayglow data. This night data would have to be shuttle induced glow for any CO lines that were observed. There are no known excitation mechanisms which could cause CO to emit radiation in the night time mesosphere. The chemical lifetime of CO is very short and therefore it will

Table 11. Conversion of slant path intensities to vertical density height profiles.

	Measured Slant Path Intensities ($\frac{photon}{cm^2 sec}$)		Vertical Density Profile (cm^{-3})	
Height	Run 1	Run 2	Run 1	Run 2
88	2760		1.18×10^9	
90	1270		5.4×10^8	
92	1549		6.6×10^8	
94	2000		8.6×10^8	
96	593		2.5×10^8	
98	668	219	2.9×10^8	9.4×10^7
100	1487	416	6.4×10^8	1.8×10^8
102	1196	607	5.1×10^8	2.6×10^8
104		1233		5.3×10^8
106		213		9.1×10^7
108		569		2.4×10^8
110		538		2.3×10^8
112		5210		2.2×10^9

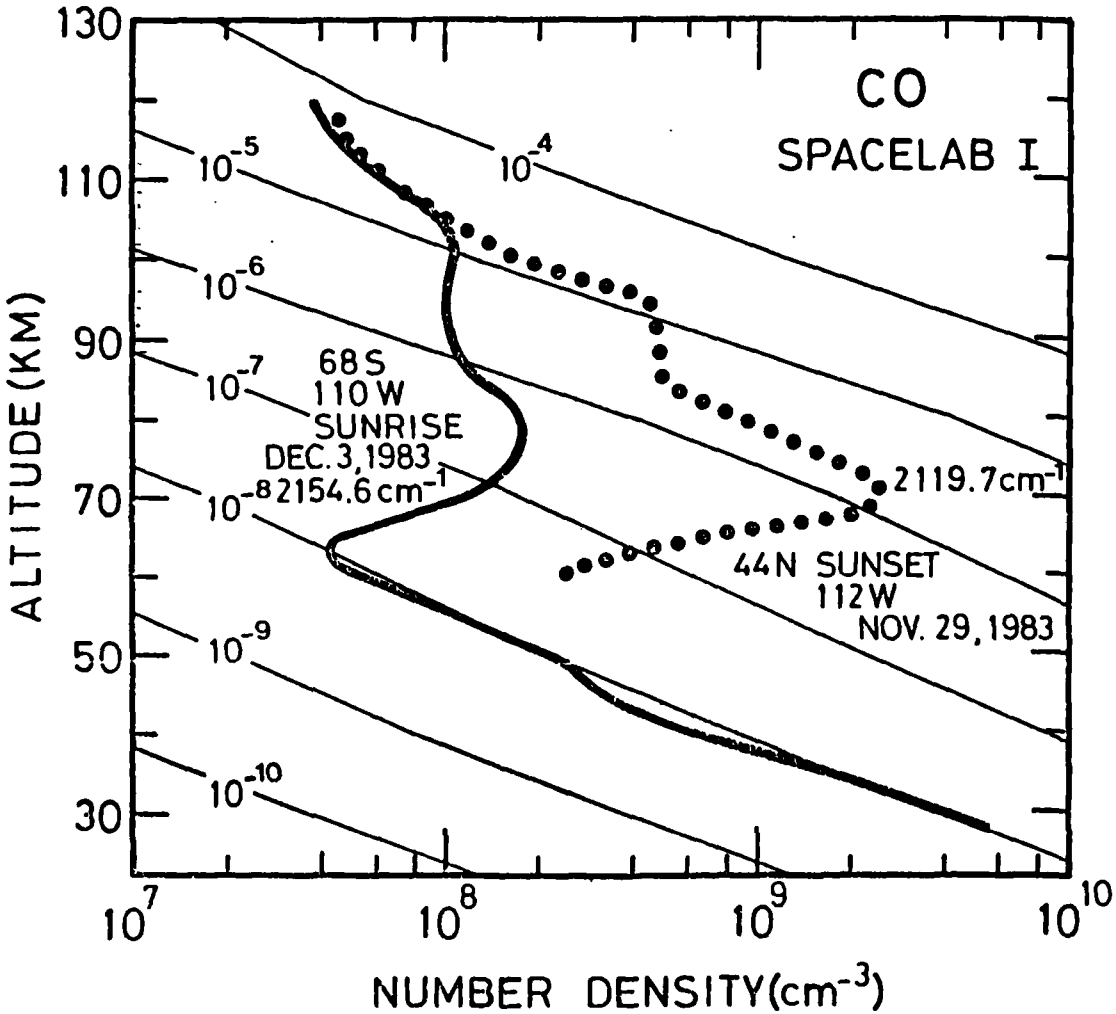

Figure 30. Number density of CO_2 and CO in molecules per cm³ versus altitude using two different CO_2 absorption lines and the $^8P_6$ CO line. The nearly parallel lines represent constant volume mixing ratios from 3×10^{-8} to 3×10^{-4}. (Lippens, et al., 1984)

not be able to hold its energy until nightfall and then radiate. This only leaves three possible excitation mechanisms for CO all of which are caused by the shuttle.

The features present on the spectra are inconsistent in that intensities vary greatly from the first spectrum (Fig. 31) to the next spectrum (Fig. 32). This is not normally associated with molecular emission features. It is not thought that these features could be due to thermal noise within the ISO. However, we can investigate the distribution source of these features using the spatial information in the imaged spectra.

To check for thermal noise, two of the brighter lines in each spectrum were broken down into the eight spatial lines. This will indicate if the line's intensity is extended or of a point source nature. If all of the intensity contribution for this line is contributed in one spatial element, then the feature is due to the energy from a localized source.

The two features examined in the first spectrum occur at 2900 Å and 3120 Å and for the second spectrum occur at 2460 Å and 3670 Å. Each of these features are shown in their eight spatial lines as follows:

2900 Å	Figure 33
3120 Å	Figure 34
2460 Å	Figure 35
3670 Å	Figure 36

Energy contributions to the 2900 Å line are apparent in steps, Figure 33-2, 3, 4, 7, 8. This is very apparent in Figure 33-2

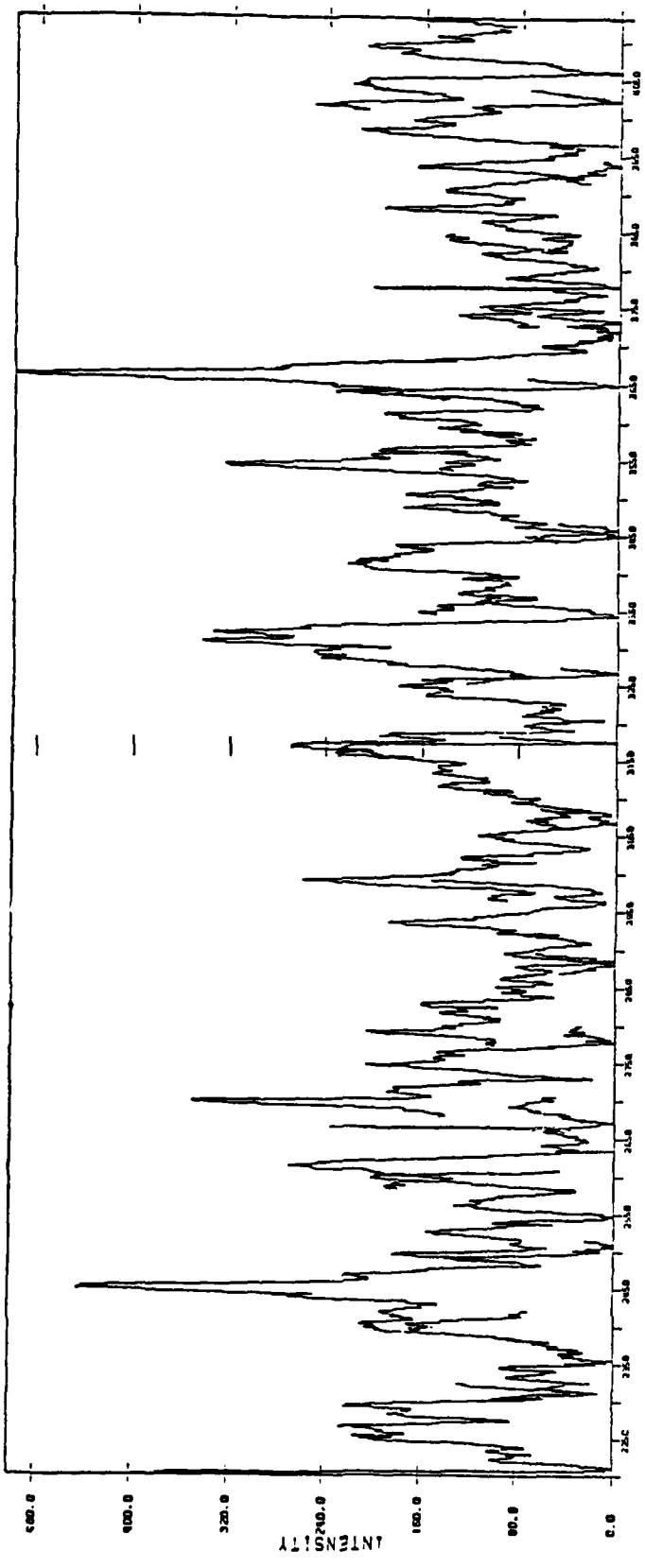

Fig. 31. The first spectra of ISO night glow data.

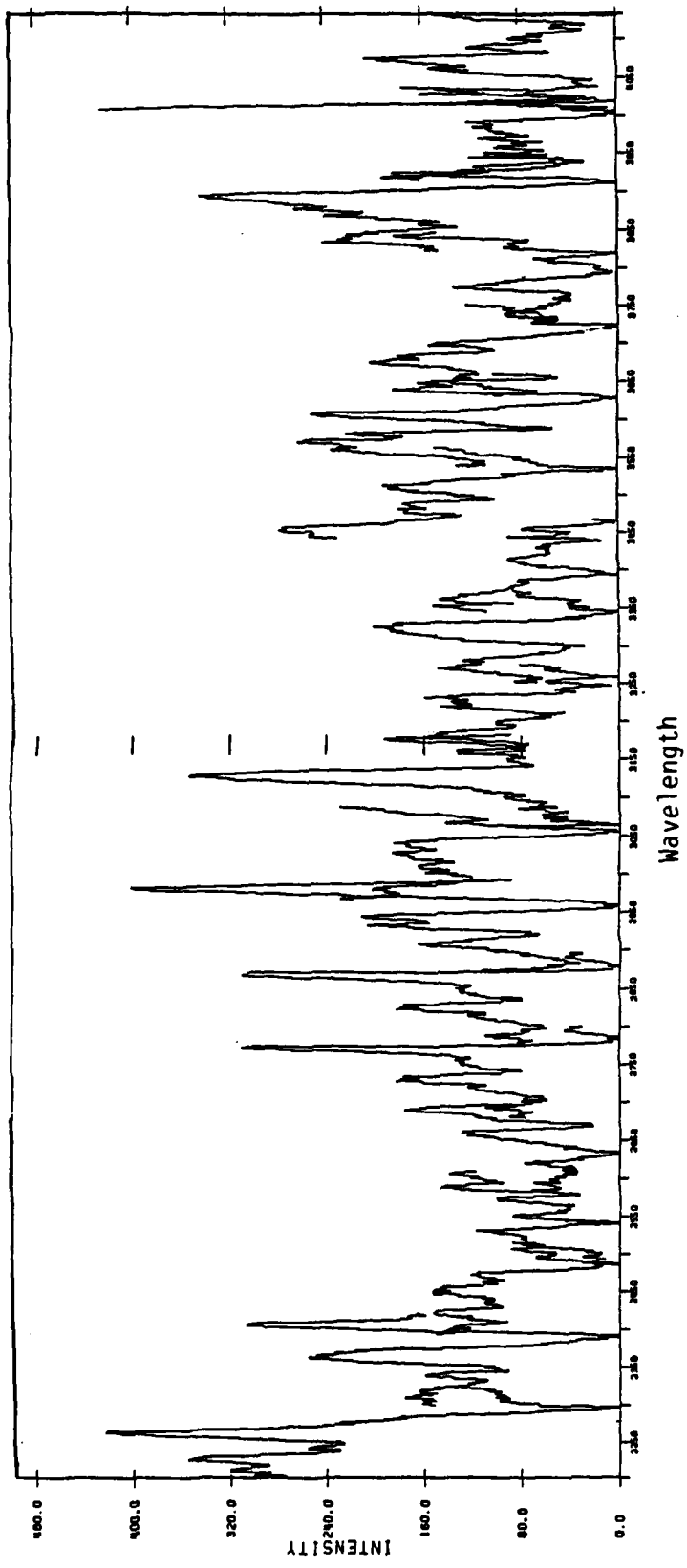

Fig. 32. The second spectra of ISO night glow data.

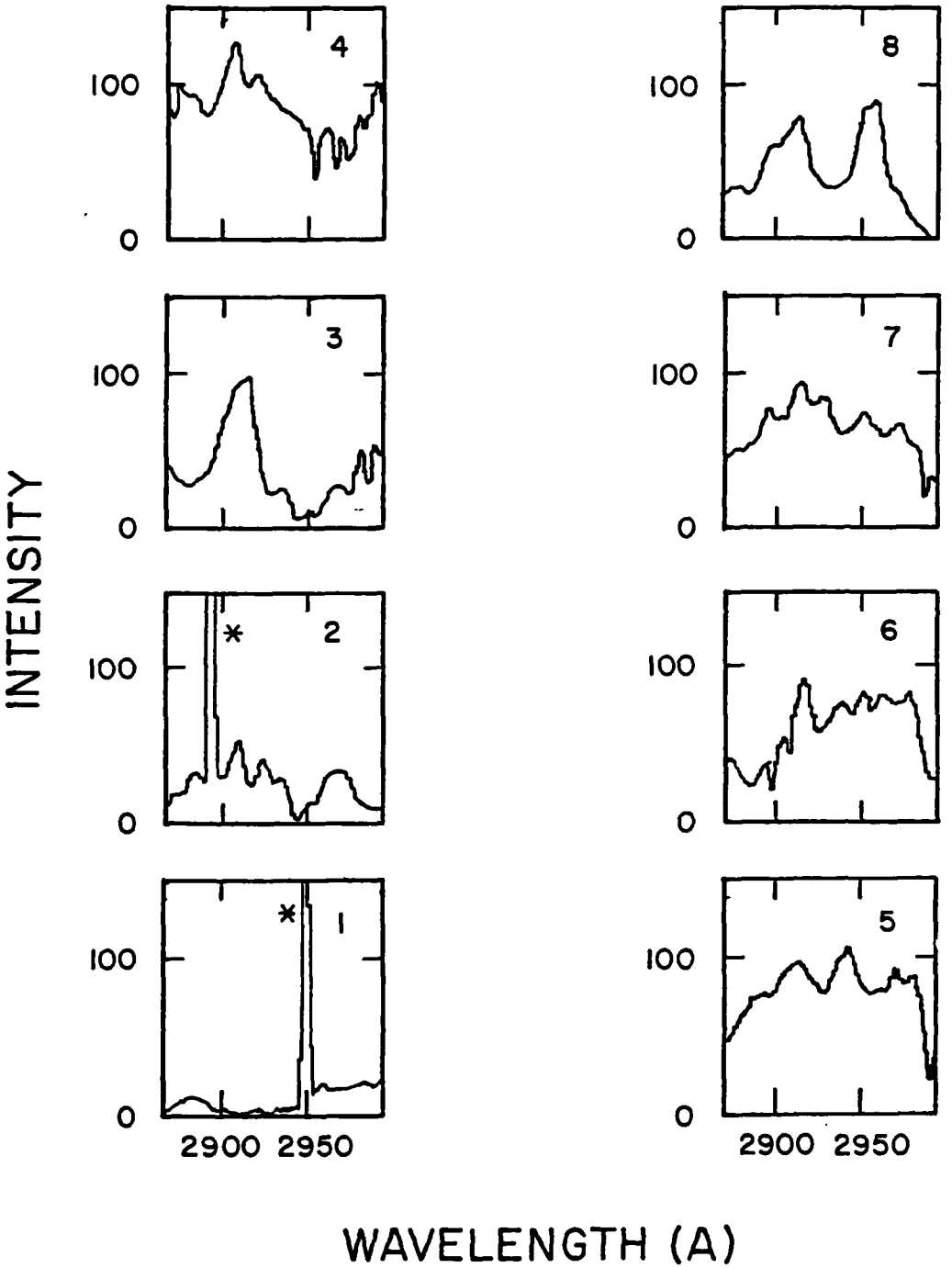

Fig. 33. Eight spatial (1-8) representations of ISO night glow data occurring at 2900 Å.

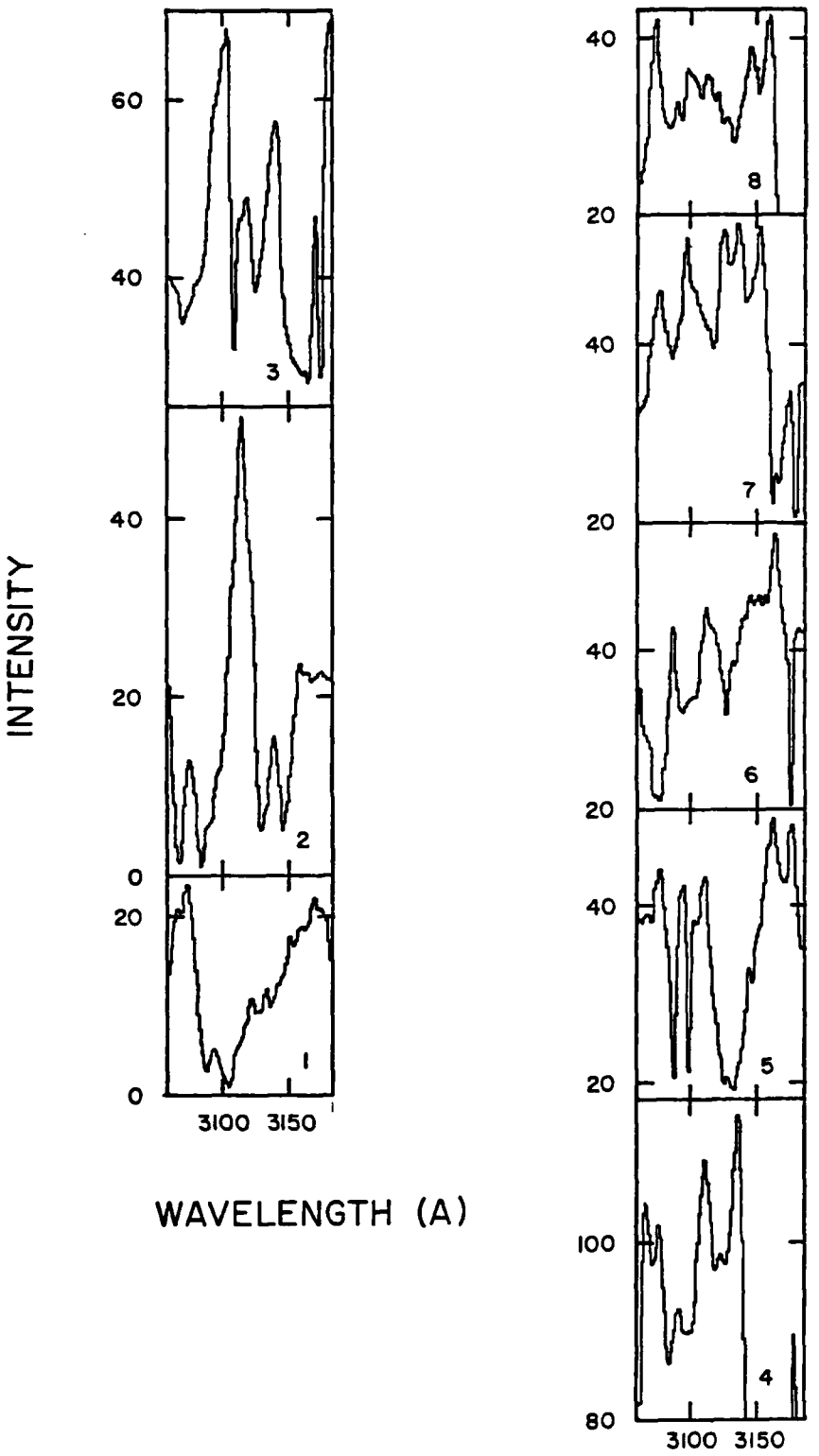

Fig. 34. Eight spatial (1-8) representations of ISO night glow data occuring at 3120 Å.

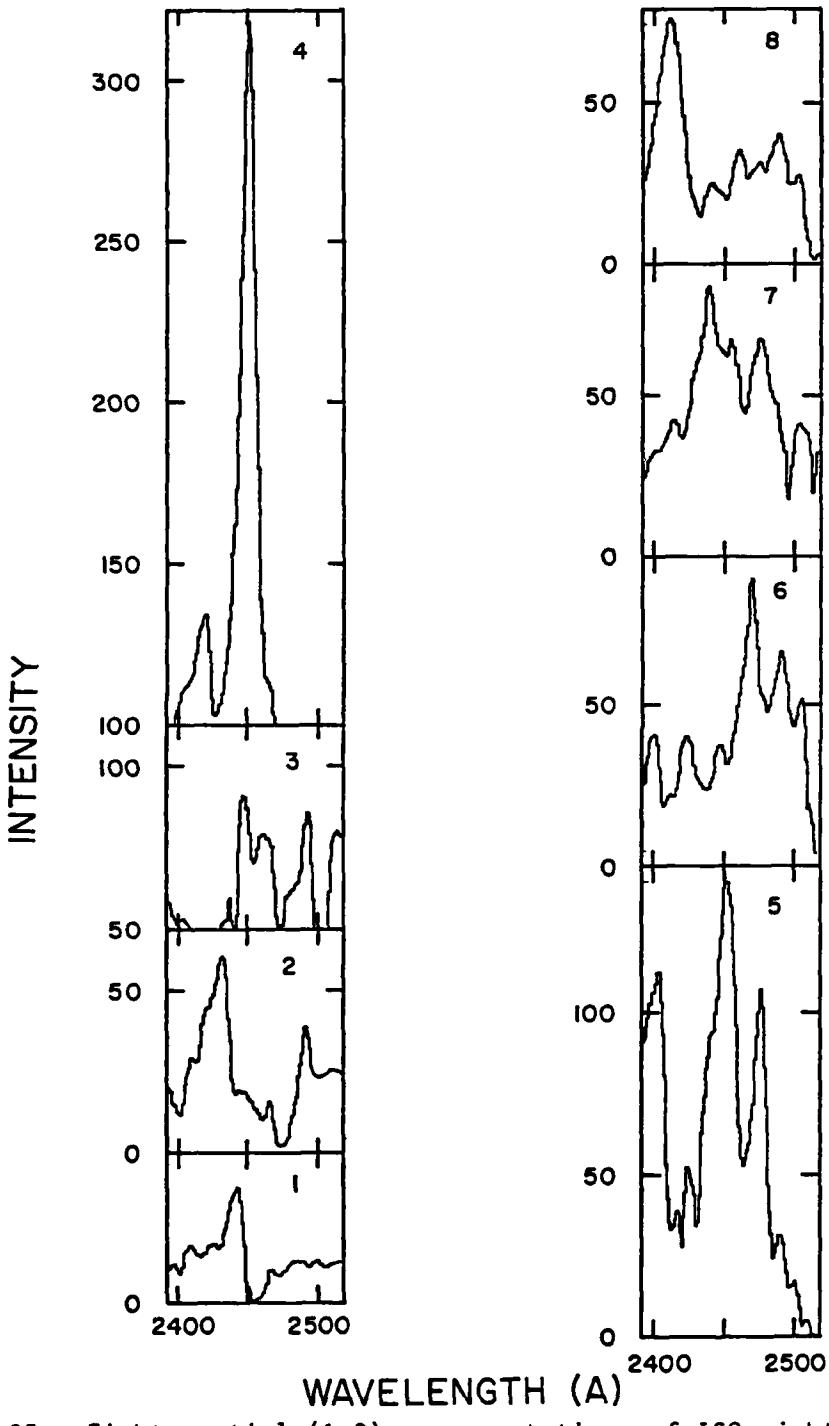

Fig. 35. Eight spatial (1-8) representations of ISO night glow data occurring at 2460 Å.

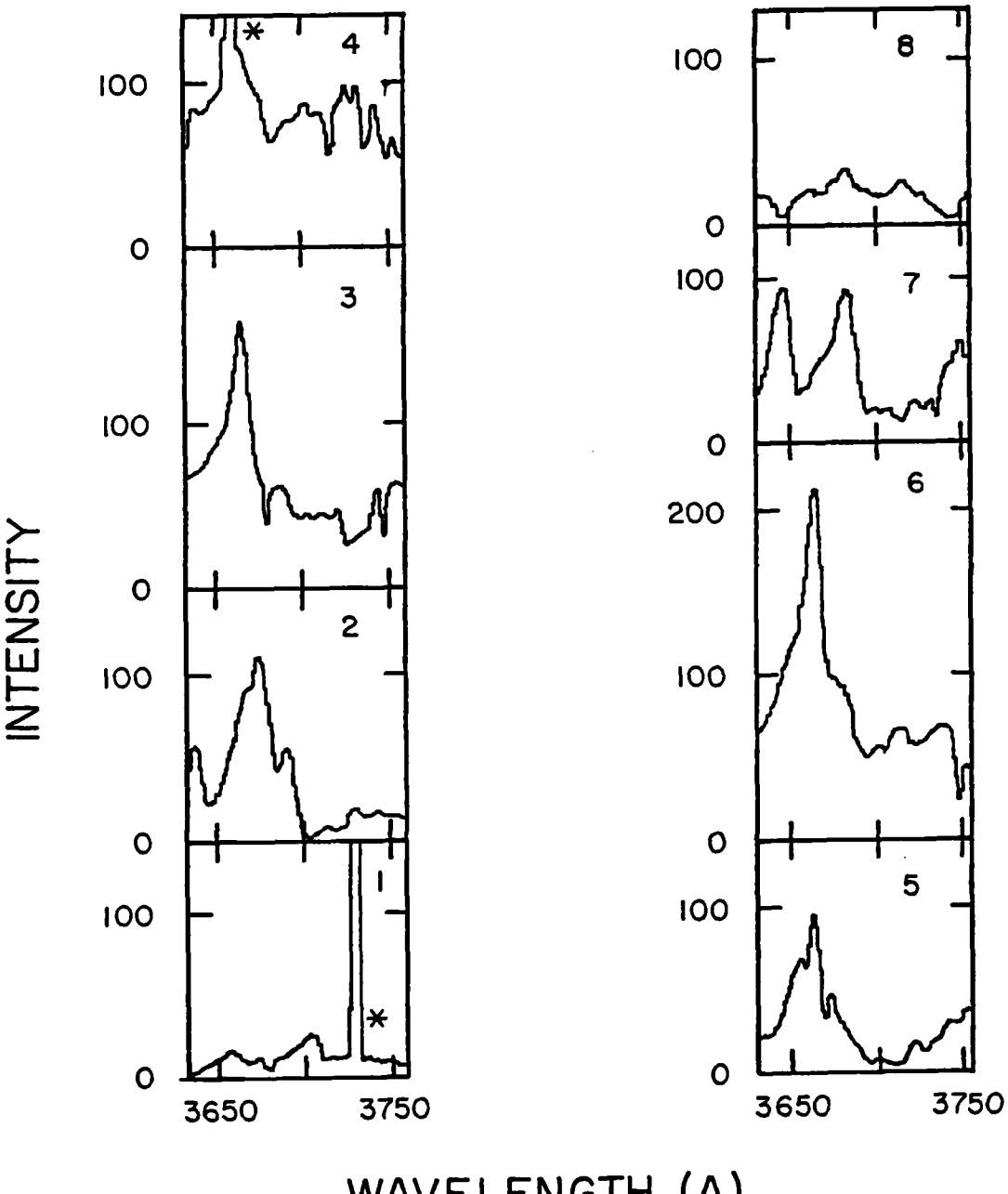

Fig. 36. Eight spatial (1-8) representations of ISO night glow data occurring at 3670 Å.

which shows a spike which appears to be noise on the telemetry. For the 3120 Å feature, Figure 34-2, 3, 4, 5, 7, and 8 shows the signal in varying intensities but does not display any thermal noise spikes. The 2460 Å feature which occurs on the second spectrum (Fig. 32) has energy inputs from Figure 35-2, 3, 4, 5, 7 and 8. Again, there is no indication of a noise spike. The final emission line considered (3670 Å) displays a signal in Figure 36-2, 3, 4, 5, and 6 with a telemetry noise spike as shown on part 4.

Only two of the features examined above contain noise spikes [the 2900 Å feature in spectrum one (Fig. 31) and the 3670 Å line in spectrum two (Fig. 32).] Although this partially explains these two features, it does not account for the 3120 Å line (spectrum one) and the 2460 Å line (spectrum two). In fact these telemetry noise spikes do not contribute 100 percent of the intensity needed to produce the 2900 Å and 3670 Å lines. However, because the signals which are measurable are not clearly present in all eight height lines, it is unlikely that they all represent molecular or atomic emissions. It has been suggested that these lines are produced by several mechanisms such as cosmic radiation, high energy electrons/protons hitting the detector, a star being observed over the limb of the earth or particulates in the field of view (M. Torr, 1985). A still, low light photograph taken on the Spacelab I flight with the ISO supports the possibility of particulates in the field of view of the instrument (see Figure 37). These particulates could cross only a few of the ISO's spatial

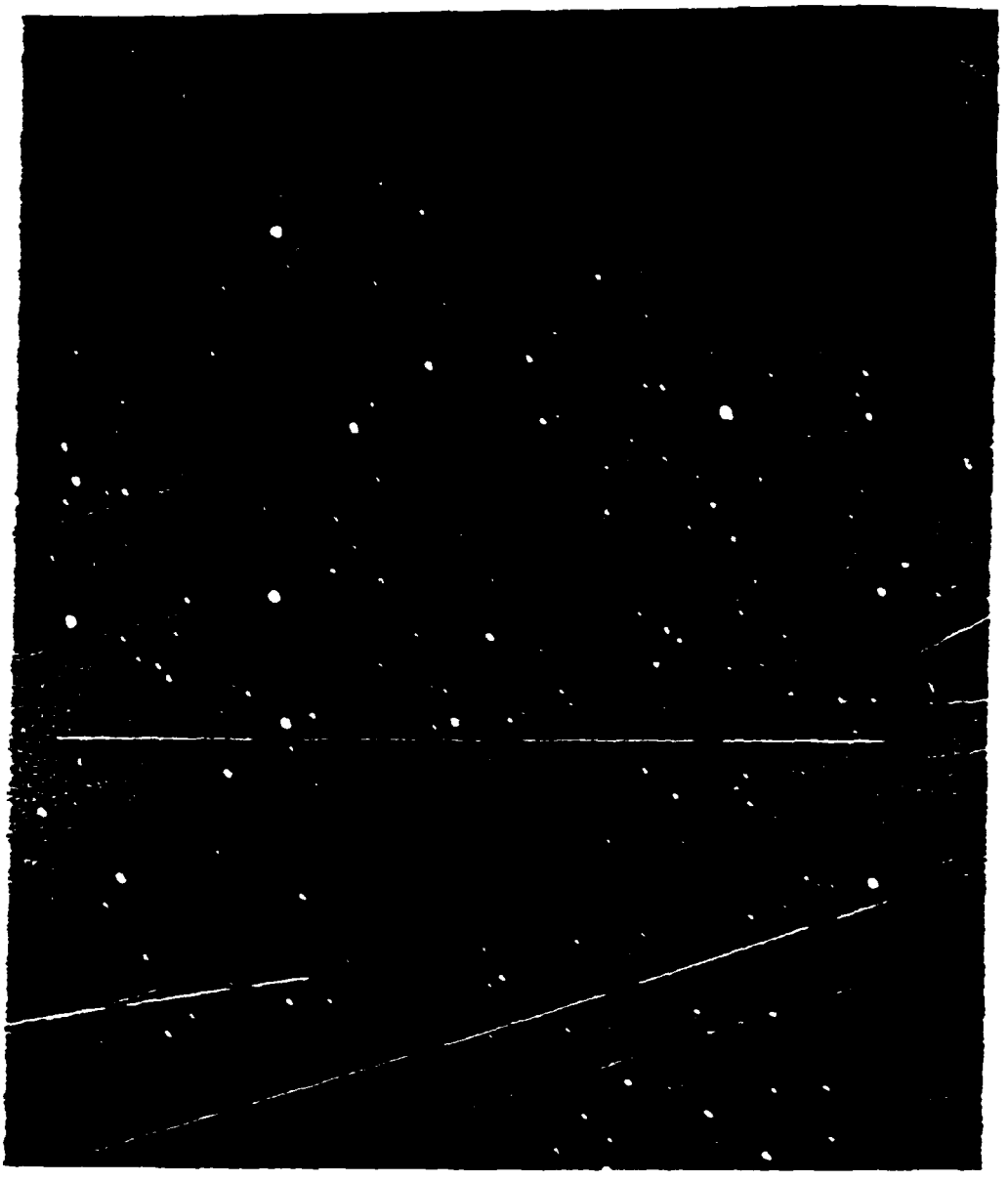

Figure 37. Still low light photograph taken on board Spacelab I which shows particulates streaming over shuttle instrumentation.

elements. Thus explaining many of the features which were shown on Figures 33, 34, 35 and 36, and were only detectable on a few of the spatial elements of the spectra. Whether either, or all of these is correct needs to be determined, which is beyond the scope of this thesis. Because these features do not appear due to molecular emission, further data analysis is not necessary.

CONCLUSIONS AND RECOMMENDATIONS

Conclusions

This study attempted to determine if the ISO could measure carbon oxide UV emission in both the dayglow (mesosphere) and shuttle induced glow. Through brighteness predictions and photochemical modeling, only one carbon oxide band (CO fourth positive) was found to be intense enough to be measurable by the ISO. After comparing all of the CO fourth positive lines (which appeared on the spectrum) to the NO gamma, NO delta, and N_2 LBH bands, only three remained which were considered pure CO fourth positive lines. The three lines were then broken down into intensity height profiles. These height profiles were compared to a brighter line (produced by the NO gamma 4,0 line). Because this was not conclusive the measured intensity values for the ISO were converted to vertical density height profiles and compared to CO measurements taken in the infrared (Lippens et al., 1984). The graphs on Figure 33 show that the ISO is measuring CO in the mesosphere.

The night data collected by the shuttle initially appeared to have some very strong features. However, on closer inspection of the data, there appeared to be differences in intensities between the two separate spectra. This is possibly an indication of thermal noise. To check for this, two bright features (from each spectrum) were broken down into their height lines. If there

was thermal noise, it would only be present on one spatial line because of the physical distance the thermal photon covers when it hits the detector. Two of the studied lines did show thermal noise. However, both the lines which showed thermal noise and the two which did not show thermal noise, had signals on four or five of the lines. This is not thermal noise and cannot be a molecular emission feature. It has been suggested that these signals are caused by cosmic radiation, high energy electron/protons impinging on the ISO detector, possibly a star being observed over the limb of the earth or most likely particulates passing in the field of view of the ISO. Regardless of this, it currently cannot be determined if the ISO is measuring carbon oxide emission induced by the shuttle.

Recommendations

Two major problems with the analysis of the mesospheric data occurred with the data collection and sensitivity level of the ISO. The first problem resulted when one of the spectrometers was damaged and collected noise. There were problems with a spurious signal which overpowered the portion of the spectrum where the brightest CO fourth positive bands occurred. The second problem resulted from the ISO's signal to noise sensitivity requiring bright band emissions which the CO and CO^+ bands could not produce. The first recommendation is to collect much more data which would include the spectral range from 2200 Å to 4100 Å and attempt to compensate for the spurious signal which overpowered the brightest of the CO fourth positive bands. The second recommendation

requires the ISO's sensitivity threshold to be dropped from 30 R/Å to 10 R/Å. This would allow many more carbon oxide lines to be observed increasing the possibility that several more carbon oxide lines could be remotely measured in the mesosphere, thus increasing our understanding of mesospheric process (both physical and chemical).

To study the shuttle induced glow, first an understanding of the unexplained features which appear on both spectra must be investigated. Any or all of the causes for these features should be eliminated or compensated for. This includes cleaning up the shuttle environment so that particulates and exhaust contaminants will not interfer with scientific optical instrumentation. Collecting more data examples and compensating for stars which appear in the ISO's field of view would be very helpful. Further instrument cooling and shielding could help eliminate thermal noise and noise caused by energetic electron/proton penetration. Then perhaps some carbon oxide features could be measured.

LITERATURE CITED

Arnold, J.O., E.E. Whiting and G.C. Lyle. 1969. Line by Line Calculation of Spectra From Diatomic Molecules and Atoms Assuming a Voigt Line Profile. J. Quant. Spectrosc. Radiat. Transfer. 9:775-798.

Barth, Charles A. 1965. Ultraviolet Spectroscopy of Planets. JPL Tech. Rep. No. 32-822:1-38.

Barth, C.A., C.W. Hard, J.B. Pearce, K.K. Kelly, G.P. Anderson, and A.I. Stewart. 1971. Mariner 6 and 7 Ultraviolet Spectrometer Experiment: Upper Atmosphere Data. J. Geophys. Res. 76(10):2213-2227.

Conway, Robert R. 1981. Spectroscopy of the Cameron Bands in the Mars Airglow. J. Geophys. Res. 86(A6):4767-4775.

Donn, B., M. Mumma, W. Jackson, M. A'Hearn and R. Harrington. 1974. The Study of Comets, Part 2. The Proceedings of IAU Colloquium No. 25, CO-Sponsored by COSPAR National Aeronautics and Space Administration, Washington, D.C., NASA SP-393:773-795.

Durrance, Samuel T. 1981. The Carbon Monoxide Fourth Positive Bands in the Venus Dayglow I. Synthetic Spectra. J. Geophys. Res. 84(A11):9115-9124.

Feldman, P.D. 1978. A Model of Carbon Production in a Cometary Coma. Astron. Astrophys. 70:547-553.

Feldman, P.D. and W.H. Brusil. 1976. Carbon Production in Comet West 1975n. Astrophys. J. 209:L45-L48.

Festou, M.C., P.D. Feldman and H.A. Weaver. 1982. The Ultraviolet Bands of the CO_2^+ Ion in Comets. Astrophys. J. 256:331-338.

Fox, J.L. and A. Dalgarno. 1979. Ionization, Luminosity and Heating of the Upper Atmosphere of Mars. J. Geophys. Res. 84:7315-7333.

Goody and Walker. 1972. Evolution of the Atmosphere. Prentice-Hall Inc., Englewood Cliffs, N.J.

Hays, P.B. and J.J. Olivero. 1970. Carbon Oxide and Monoxide Above the Troposphere. Planet. Space Sci. 18:1729-1733.

Hessen, James E., Kurt Dressler. 1965. Absolute Transition Probabilities in the Ultraviolet Spectrum of CO. J. Astrophys. 142:389-390.

Jain, D.C. and R.L. Sahni. 1966. Transition Probability Parameters of the Band Systems of CO^+. J. Quant. Spectrosc. Radiat. Transfer. 6:705-715.

James, C. Thomas. 1971. Transition Moments, Frank-Condon Factors, Lifetimes of Forbidden Transitions. Calculation of Intensity of the Cameron Systems of CO. J. of Chem. Phys. 55(8):4118-4124.

Joshi, K.C., V.D.P. Sastri and S. Parthasarathi. 1966. Absolute Transition Probabilities, Oscillator Strengths, and Electronic Transition Moments for the First Negative System of CO^+. Journ. Quant. Spectrosc. Radiat. Transfer. 6:215-219.

Lippens, C. C. Muller, J. Vercheral, M. Ackerman, J. Laurent, M. Plamaitre, J. Besson and A. Girard. 1984. Trace Constituents Measurements Deduced From Spectrometer Observation Onboard space Lab. Belgisch Instituut Voor Ruimte-Aeronomie. 1-12.

Murad, Edmond. 1985. Implications of Mass Spectrometric Measurements on space Shuttle. Planet. Space Sci. 33(4):421-423.

Pearse, R.W.B. and A.G. Gaydon. 1984. Identification of Molecular Spectra. Chapman and Hall, London.

Torr, Douglas G. 1985. The Photochemistry of Atmospheres Earth, the Other Planets and Comets. Academic Press Inc.: 165-278.

Torr, Marsha R. 1985. Class Notes from Aeronomy 701, 702, 703. Utah State University, Logan, Utah.

Torr, Marsha R., R. W. Basedow and P.G. Torr. 1982. Spectroscopic Imaging of the Thermosphere from the Space Shuttle. Applied Optics. 21(22):4130-4145.

Torr, Marsha R. and D.G. Torr. 1984. Atmospheric Spectral Images. Science 225:169-171.

Whiting, Ellis E., James O. Arnold and Gilbert C. Lyle. 1969. A Computer Program for a Line-by-Line Calculation of Spectra From Diatomic Molecules and Atoms Assuming a Voigt Line Profile. Ames Research Center Moffett Field, California, NASA Tech. Note D-5088: 1-15.

Yung, Yuk Ling, Darrel F. Strobel, Tan Ying Kong and Michael B. McElroy. 1971. Photochemistry of Nitrogen in the Martian Atmosphere. Icarus. 30:26-41.

END

DTIC

5-86